A Bayesian approach to the deconvolution of $^{40}Ar/^{39}Ar$ data from mineral mixtures

John N. Carter [1,*], Marissa M. Tremblay[2], and Darren F. Mark[1,3]

1. Scottish Universities Environmental Research Centre, Rankine Avenue, East Kilbride, G75 0QF, United Kingdom
2. Department of Earth, Atmospheric, and Planetary Sciences, Purdue University, West Lafayette, IN, 47907, United States
3. School of Earth & Environmental Sciences, University of St Andrews, St Andrews, KY16 9AJ, United Kingdom

*Corresponding author

Email addresses: j.carter.1@research.gla.ac.uk (J.N. Carter)
tremblam@purdue.edu (M.M. Tremblay)
darren.mark@glasgow.ac.uk (D.F. Mark)
Phone number: +44 (0) 791-719-1205 (J.N. Carter)

Keywords: $^{40}Ar/^{39}Ar$ geochronology; Bayesian; Markov Chain Monte Carlo; mixture modeling; planetary geochronology; provenance

ABSTRACT

$^{40}Ar/^{39}Ar$ geochronology is a powerful technique for dating geological events and processes on timescales from hundreds to billions of years. Most $^{40}Ar/^{39}Ar$ datasets are collected from analysis of single mineral phases or phenocryst-free groundmass that cooled rapidly following a volcanic eruption, which can allow for straightforward interpretation of $^{40}Ar/^{39}Ar$ age spectra. However, $^{40}Ar/^{39}Ar$ age spectra from mixtures of multiple minerals and/or multiple age components are often complex. In such situations, interpretations commonly used for single mineral phases are inappropriate and will result in geologically spurious conclusions. Here, we present a Bayesian method for the analysis and interpretation of $^{40}Ar/^{39}Ar$ step-heating spectra that result from mixing of multiple components, where a component is defined by both its age and mineral composition. We test the efficacy of this Bayesian approach using a suite of case studies. Two of these case studies utilize $^{40}Ar/^{39}Ar$ data from laboratory-prepared mixtures, which we use to explore how the composition, age, and number of components in a mixture, as well as our prior knowledge of these parameters, influence the model results. We also present an application-based case study in which we use plausible compositions and ages from a past Mars landing site to generate a synthetic $^{40}Ar/^{39}Ar$ dataset, which we then deconvolve using our Bayesian approach. We discuss modifications to our method that could improve the model's precision and outline geologic applications of our Bayesian approach in terrestrial and extraterrestrial settings that would permit the extraction of a greater amount of temporal information.

1. INTRODUCTION

The $^{40}Ar/^{39}Ar$ method is widely used to date geological events that span the entire ca. 4.6 Ga of our Solar System's history (e.g., Renne et al., 1997; Renne et al., 2000; Preece et al., 2018). In most applications of the $^{40}Ar/^{39}Ar$ method, single mineral phases or phenocryst-free groundmass from igneous or metamorphic rocks are selected for analysis following standard sample preparation techniques such as acid leaching, magnetic separation and picking under optical microscope (e.g., McDougall and Harrison, 1999). Isolating mineral phases for $^{40}Ar/^{39}Ar$ dating often, though not always, allows for straightforward interpretation of the resulting datasets.

$^{40}Ar/^{39}Ar$ data from step degassing measurements are typically presented and interpreted on an age spectrum plot, where the $^{40}Ar^*/^{39}Ar$ ratio ($^{40}Ar^*$ denoting radiogenic ^{40}Ar derived from the decay of ^{40}K) observed during each heating step, which is proportional to the apparent step age,

is plotted as a function of cumulative ^{39}Ar release (Merrihue and Turner, 1966). If a reproducible $^{40}Ar^*/^{39}Ar$ ratio (heating steps that are statistically indistinguishable at 2 sigma) and therefore age are found in over 60% (Fleck et al., 1977) of the continuous step degassing of a sample, we typically infer that the sample cooled geologically instantaneously, resulting in an ultimately spatially uniform distribution of $^{40}Ar^*$. In such cases, we identify concordance from the age spectrum as a plateau. Once a plateau has been identified, we report the $^{40}Ar/^{39}Ar$ age of that sample as a weighted mean by inverse variance of the steps comprising the plateau (McDougall and Harrison 1999), and this $^{40}Ar/^{39}Ar$ age is typically interpreted to be geologically meaningful (e.g., an eruption age for a volcanic rock).

We can also make geologic inferences about processes affecting the distribution of ^{40}Ar and therefore the $^{40}Ar/^{39}Ar$ age spectra in single-component samples. For example, diffusive loss of $^{40}Ar^*$ for samples with single diffusion domains manifests as monotonically increasing steps in an $^{40}Ar/^{39}Ar$ age spectrum (Turner, 1968). Depending on the setup of the step degassing experiment, it is possible to calculate the kinetics of Ar diffusion in a sample from the degassing of reactor-induced ^{39}Ar or ^{37}Ar, which allows us to model the geologic time-temperature history that would result in the observed $^{40}Ar/^{39}Ar$ release pattern (e.g., Foland, 1994, Cassata et al., 2010). Recoil loss and excess ^{40}Ar also affect age spectra in predictable ways. Recoil loss of reactor-induced ^{39}Ar normally manifests as initial steps with high $^{40}Ar^*/^{39}Ar$ and old ages, due to ^{39}Ar loss from the edges of mineral grains, and lower $^{40}Ar^*/^{39}Ar$ and younger ages for later high-temperature steps, resulting from the redistribution of ^{39}Ar (Onstott et al., 1995). If multiple diffusion domains are present, this redistribution is often interpreted as transport of ^{39}Ar out of K-rich diffusion domains and into relatively K-poor, more retentive domains (Onstott et al. 1995). Extraneous ^{40}Ar ($^{40}Ar_{ex}$), which is thought to be either inherited argon from older grain contamination or non-radiogenic ^{40}Ar contamination (Kelley, 2002), typically manifests as saddle shape age spectra with relatively high $^{40}Ar/^{39}Ar$ ratios at the beginning and end of step heating (Lanphere and Dalrymple, 1976).

There are a number of potential applications of $^{40}Ar/^{39}Ar$ geochronology, however, for which mineral separation is not feasible. For example, $^{40}Ar/^{39}Ar$ dating is frequently utilized for provenance analysis of sediments and sedimentary rocks in tectonic and paleoclimatic studies (Copeland and Harrison 1990; Hemming et al., 1998; Singer et al., 2004), but at present is largely restricted to coarse-grained sediments for which individual mineral grains can be obtained. Such isolation of individual grains is difficult for fine-grained materials and even if such

a separate could be produced, the amount of material would still preclude single grain analyses. Bulk sediment provenance analysis of fine-grained sediments via $^{40}Ar/^{39}Ar$ geochronology has been used to understand source changes through time in marine or lacustrine depositional environments (e.g., VanLaningham et al., 2006), but owing to a lack of interpretive frameworks, interpretations are restricted to simply identifying changes in source region through time and not determining the ages of different components. Extraterrestrial meteorite samples are another example where $^{40}Ar/^{39}Ar$ geochronology of multiple mineral phases is often required due to very small sample sizes, but also desirable because different mineral phases will have different temperature sensitivities and potentially record different thermal events in a meteorite's history (e.g., Cassata et al., 2010; 2018). Similarly, potential *in situ* rover-based $^{40}Ar/^{39}Ar$ geochronology on future missions to Mars, the Moon or other rocky bodies (e.g., Morgan et al., 2017) would require analyses of multiple mineral phases as sample preparation has been limited to simple sieving (Farley et al., 2014).

In situations where single mineral components cannot be isolated, conventionally used interpretations of $^{40}Ar/^{39}Ar$ spectra are inappropriate. This has been demonstrated by a number of studies using artificial mixtures to explore the impact of multiple components on age spectra. Rex et al. (1993) showed that mixing a hornblende with a younger biotite that was less retentive of Ar produced a monotonically increasing age spectrum, similar to the shape conventionally interpreted to reflect Ar diffusive loss during slow cooling (Turner, 1968). Kula et al. (2010) mixed two muscovite samples and two biotite samples, each of different ages. Individually, muscovite and biotite samples yielded flat age spectra consistent with an interpretation of rapid cooling. However, when mixed and step heated, the muscovite samples yielded relatively flat intermediate-age plateaus with plateau age varying as a function of the mixing proportion, while the biotite mixtures yielded highly complex and discordant age spectra. In exploring the range of effects that degassing multiple mineral components simultaneously has on $^{40}Ar/^{39}Ar$ age spectra, these studies and others (discussed below) demonstrate that the conventional method of interpreting an age 'plateau' from an $^{40}Ar/^{39}Ar$ age spectrum is erroneous. To extend $^{40}Ar/^{39}Ar$ to the realm of multi-component mineral mixtures it is clear that new analytical techniques are needed, in this paper we present a method based on Bayesian parameter inference to obtain the age(s) of each component in a multi-component mineral $^{40}Ar/^{39}Ar$ dataset. Firstly, we discuss prior modelling techniques to extract age information from multi-component mineral $^{40}Ar/^{39}Ar$ datasets and present our model in the methods section.

Although multi-component $^{40}Ar/^{39}Ar$ age spectra cannot be interpreted via conventional methods, a number of different approaches have been attempted to maximise information recovery from the complicated age spectra resulting from analysis of mixtures. Among these, several are semi-quantitative or descriptive in nature. For example, Gillespie et al. (1982) model how, in a mixture of two minerals that have substantially different activation energies, the Ar from the two minerals is effectively separated by detailed step heating analyses. Gillespie et al. (1982) illustrate their model with both a theoretical age spectrum and an age spectrum of mixed felsic minerals from a partially degassed granitoid xenolith in basalt. The application of the model in Gillespie et al. (1982) is limited to qualitative analysis of the two-component age spectrum with no direct fit of the data and no recovery of age information. Forster and Lister (2004) proposed a method to interpret complex age spectra from two-component mixtures of micas that involves statistically analysing age spectra for frequently measured ages (FMA) and using these FMAs to define asymptotes in the spectra. In their interpretation, an upward-converging age asymptote represents the minimum age of one component, while a downward-converging asymptote represents a maximum age of the other. While this method could be used to infer the presence of multiple components, it only provides an upper or lower bound on the age of any component; in cases where components of the same phase are mixed, resulting in intermediate plateau ages, the recovered information may have no geological meaning (e.g., Kula et al., 2010). VanLaningham and Mark (2011) created synthetic mixtures of well-constrained $^{40}Ar/^{39}Ar$ mineral standards, including Taylor Creek Rhyolite sanidine (TCRs), Alder Creek sanidine (ACs), Heidelberg biotite (HD-B1). The authors showed that the shape of the age spectra resulting from stepwise degassing of these samples could be predicted, but they do so with a great deal of prior knowledge about the different components (K concentration, $^{40}Ar/^{39}Ar$ age of the monitor minerals, Gaussian distributed release of Ar, and the mean and variance of the Gaussian release from the individual phases). VanLaningham and Mark (2011) suggest that it may be possible to invert their age spectra to solve for the ages of the individual mineral components, should enough degassing steps be conducted during sample analysis.

Quantitative numerical approaches have also been used to interpret age spectra from multi-component mixtures. Each of these approaches is rooted in the Multiple Diffusion Domain model (MDD) originally formulated by Lovera et al. (1989). The MDD model was introduced to interpret complex $^{40}Ar/^{39}Ar$ age spectra from alkali feldspars that in many ways resemble age spectra from multi-component mixtures. The MDD model assumes that individual K-feldspar crystals contain multiple diffusion domains that are non-interacting and are characterized by

different diffusion length scales (Lovera et al., 1989, Lovera et al., 2002). In the case of multi-component mixtures, different components essentially act as separate, non-interacting domains (which themselves might exhibit MDD behavior). For example, Cassata et al. (2010) used the MDD model framework to interpret $^{40}Ar/^{39}Ar$ age spectra from polymineralic samples of Martian meteorites ALH84001 and Nakhla. These authors report multi-phase MDD-type models that reproduce the ^{39}Ar and ^{37}Ar diffusivities calculated from step heating results. Cassata et al. (2010) then use these models to explore time-temperature histories consistent with the observed $^{40}Ar/^{39}Ar$ age spectra. Analogous multi-phase MDD-type models have been implemented since (e.g., Shuster and Cassata, 2015) Although Cassata et al. (2010) and subsequent studies are able to find time-temperature histories that agree with their observed age spectra, their forward modelling approach is limited by subjective choices with regards to the diffusion kinetics model fits and the range of time-temperature histories they explore. Boehnke et al. (2016) applied a multi-phase MDD type modelling approach to interpret $^{40}Ar/^{39}Ar$ spectra obtained from whole rock chips of the Jilin chondrite and the Apollo 16 lunar breccia 67514. In contrast to the forward modelling approach of Cassata et al. (2010), Boehnke et al. (2016) use a global optimization algorithm to invert both the Arrhenius plots for multi-phase MDD diffusion kinetics and the age spectra for time-temperature history. Their inversion method is able to resolve the observed age spectra and place constraints on the timing and duration of shock-related heating events. Of the existing numerical approaches to interpreting multi-component mixtures, the Boehnke et al. (2016) approach is the least restrictive in terms of number of required assumptions. Nonetheless, their approach requires highly computational processes that prevent the direct estimation of uncertainty on parameters such as age and diffusion kinetics (Boehnke et al., 2016).

In this paper we describe an approach for the deconvolution of multi-component $^{40}Ar/^{39}Ar$ age spectra using a Bayesian model. The overarching goals of the modelling are threefold: (1) to reproduce the age spectrum generated during laboratory degassing, (2) to deconvolve the Ar released from each component, and (3) to determine the age of each component. Unlike the approach of Boehnke et al. (2016), we are not performing a joint inversion of the age spectrum and the components' diffusion parameters. Rather, we are constructing a joint probability model of the cumulative ^{39}Ar release curve, defined as the cumulative fraction of ^{39}Ar released as a function of temperature, and the age spectrum, defined as the apparent $^{40}Ar/^{39}Ar$ age as a function of the cumulative fraction of ^{39}Ar released, while using prior information about the diffusion parameters. It is worth noting, however, that the Arrhenius plot from which Boehnke et

al. (2016) invert diffusion parameters is derived from the cumulative ^{39}Ar release curve that we use in our joint probability model. A strength of using the joint probability model in our Bayesian approach is that it allows for flexibility to include additional sources of information in the model, such as the K/Ca spectrum, which we discuss in more detail later.

To demonstrate the strengths and challenges of our approach, we present three case studies. In each case study we use our Bayesian inversion model to quantitatively fit observed or simulated $^{40}Ar/^{39}Ar$ age spectra and cumulative ^{39}Ar release curves and recover the ages of the individual components in the mixture. In the first case study, we reevaluate $^{40}Ar/^{39}Ar$ step-heating data from mixtures of neutron fluence monitor standards reported by VanLaningham and Mark (2011) as described above, using only prior knowledge about the number and composition of components in each mixture. The second case study utilises the mixtures of muscovite and biotite samples of different ages reported by Kula et al., (2010). We use this case study to demonstrate a limiting case for our approach, as we cannot effectively 'un-mix' the ages of components with the same composition without prior knowledge of both the mixing fraction and number of components. In the third case study, we use plausible compositions and ages for components in the Martian regolith to generate a synthetic $^{40}Ar/^{39}Ar$ age spectrum. We then use our Bayesian inversion method with reasonable priors to model these synthetic data. This case study demonstrates the utility of our method for interpreting complex $^{40}Ar/^{39}Ar$ data to obtain geologically meaningful ages from whole rock meteorite or mission-returned samples, or *in situ* on potential future planetary exploration missions.

2. METHODS

2.1 Phenomenology represented in the model

In order to develop a Bayesian approach to interpreting $^{40}Ar/^{39}Ar$ spectra from multi-component mixtures, we must first define models that represent the physical processes affecting the argon systematics in these mixtures. First, consider a single component in a mixture. For this individual component, we assume that the length scale of argon diffusion is defined by the grain size, and that the diffusion geometry can be approximated as a sphere with radius *a.* Although the assumption of a spherical geometry is a mathematical idealisation, it is a reasonable approximation for most mineral grains (Lovera et al., 1989, Harrison et al., 1991, Lovera et al., 2002, Gautheron and Tassan-Got, 2010). In addition to a spherical geometry, we also assume that diffusion is isotropic, and that Fick's second law describes the distribution of argon in the system:

$$\frac{\delta C}{\delta t} = D(T)a2\nabla 2C \quad (1)$$

Where C is the concentration of argon, t is time, D is the diffusivity, and T is temperature. A Fickian diffusion model implies that argon will move from regions of higher concentrations to regions of lower concentrations. We assume the boundary condition that the concentration C at a distance a, the grain boundary, is zero. With this condition equation 1 can be solved for the fractional loss (f) of a diffusant as derived by Crank (1975) and then discretized by Fechtig and Kalbitzer (1966).

Following on from the assumption of Fickian diffusion, we also assume that the diffusion of Ar is thermally driven and that the temperature dependence of diffusivity D can be described with an Arrhenius relationship:

$$D(T)a2 = D0a2\exp(EaRT) \quad (2)$$

Where D_0 is the frequency factor, E_a is the activation energy, R is the gas constant, and T and a are as defined above. The parameters E_a and D_0 are a function of a particular noble gas and mineral pair and control the temperature sensitivity of the system in question. In the case studies we present here, we also assume that each component of the mixture has cooled through its closure temperature over a geologically instantaneous time interval and remained a closed system since, resulting in a spatially uniform distribution of ^{40}Ar*. We also assume spatially uniform production of ^{40}Ar* and reactor-induced ^{39}Ar in individual components (i.e., no zonation of parent K). More complex process-based models can be incorporated into the Bayesian framework that we outline below. For example, we can use the same overall Bayesian framework to examine cases of a non-uniform distribution of ^{40}Ar* in individual components (e.g., due to thermally driven loss). We choose to present simple yet geologically reasonable cases in order to gain a basic understanding of the Bayesian model behavior, which could be obscured by introducing more complex processes and boundary conditions.

With these assumptions, we can predict the age spectrum and cumulative release curve for a single component with a laboratory heating schedule from equations 1 and 2, as we expect the

fractional release of $^{40}Ar^*$ and ^{39}Ar to be essentially equivalent in each heating step (e.g., Foland & Xu, 1990), assuming mass-dependent fractionation in nature is negligible. This mathematical framework for predicting the age spectrum and cumulative release curve of an individual component now allows us to consider the age spectrum and cumulative release curve for multiple components. The multi-component problem can be treated as a mixture model, where the measured data are a linear combination of the end member distributions. Similar to detrital zircon and grain size distribution models, our data are non-negative with a mixing fraction, ϕ, that must sum to one (e.g., Sambridge and Compston, 1994, Yu et al., 2016, Sharman and Johnstone, 2017). Given these constraints, the generalized equation for a multi-component cumulative release curve (equation 5) and age spectrum (equation 6) can be represented as:

$$\phi = = 1k\phi i = 1 \quad (3)$$

$$\mu = i = 1k\mu i = i = 1k\phi i\delta Fi(i = 1k\phi i\delta Fi) \quad (4)$$

$$Fs = i = 1k\phi i Fi \quad (5)$$

$$Ages = i = 1k\mu i Agei \quad (6)$$

Where Age_s and F_s are the measured $^{40}Ar^*/^{39}Ar$ age and cumulative ^{39}Ar release of a particular heating step, μ_i, ϕ_l, Age_i, δF_i, F_i are the mixing fraction, volume fraction, age, incremental release and cumulative release, respectively, of each component *i* in the mixture. Using these assumptions and physical representations for the argon systematics in multi-component mixtures, we developed a Bayesian framework to estimate the mixture fraction, diffusion kinetics, and age of each component from an observed multicomponent age spectrum and cumulative release curve as defined by equations 5 and 6.

2.2 Bayesian framework

Bayesian inference is a statistical technique that involves fitting a probability model to data in order to estimate parameters in the model (Gelman et al., 2013). Central to Bayesian inference is Bayes theorem (Eq. 4) which states that the posterior probability $P(\theta|y)$, or the probability of a model parameter θ given the data y, equals $P(y|\theta)$, the likelihood of the data given the model parameters, multiplied by the prior probability of the model parameter, $P(\theta)$, and divided by the probability of the data, $P(y)$.

$$P(y\theta) = P(y|\theta)P(\theta)P(y) \tag{7}$$

The probability of the data P(y), also known as the evidence, is the integration of the model probability across the entire model parameter space. The calculation of $P(y)$ is often intractable for problems with many variables requiring very high dimensional integrals. However, because $P(y)$ is a normalising constant that simply scales the posterior probability, Eq. 4 can be recast as a proportionality relationship given as:

$$P(\theta|y) \propto P(y|\theta)P(\theta) \tag{8}$$

The advantage of the Bayesian approach is that our initial knowledge about model parameters are incorporated in probability density functions we call priors $P(\theta)$. In cases where we know very little about the true value of a model parameter θ, we can give that parameter a highly uninformed prior probability distribution; in cases where we have physical constraints on θ, we can incorporate this information into $P(\theta)$. We obtain an estimate of the model parameters (the posterior), by updating our initial knowledge (the prior ($P(\theta)$) conditional on our observations (the likelihood $P(y|\theta)$) and by drawing samples from the posterior ($P(\theta|y)$).

For the multi-component $^{40}Ar/^{39}Ar$ deconvolution problem, our observed data y are the age spectrum and cumulative release curve obtained from a laboratory degassing experiment. Our model parameters, θ include the activation energy E_a, frequency factor D_0, and grain size a, for Ar diffusion in each component, the age of each component *Age*, and the volume fraction, ϕ.

The Bayesian proportionality relationship for the multi-component $^{40}Ar/^{39}Ar$ problem is as follows:

$$PEai, Doi, Agei, ai, \phi iy \propto PyEai, Doi, Agei, ai, \phi iP(Eai, Doi, Agei, ai, \phi i) \quad (9)$$

where *i* represents each component in the mixture. We follow Gallagher et al. (2012) by adopting a sum of squares for our likelihood function for both the age spectrum (Eq. 11) and cumulative release curve (Eq. 12) observations. These are expressed as follows:

$$L1 = -12i=1N(obs1i - model1i\sigma 1i)2 \quad (10)$$

$$L2 = -N2\ln 2\pi - N2\ln\sigma 2i2 - 12\sigma 2i2i=1N(obs2i - model2i)2 \quad (11)$$

For the likelihood of the age spectrum observation *L1* (given in Eq. 10), obs_{1i} is the observed age, $model_{1i}$ is the model predicted age, and σ_{1i} is the error in the observed age for each experiment time-temperature step *i*. In the case of the cumulative release curve, we define our likelihood to take the form of a normal distribution given by Eq. 11 (*L2*), wherein obs_{2i} is the observed cumulative ^{39}Ar release, $model_{2i}$ is the model-predicted cumulative ^{39}Ar release, and σ_{2i} the model error for the cumulative ^{39}Ar release. The total likelihood of the model is calculated by summing *L1* and *L2*. Given the way in which we define both likelihoods, the age spectrum likelihood typically carries the dominant weight in the likelihood summation (*L1* + *L2*). This is illustrated in Figure 5.

To predict the observed age spectrum and cumulative release curve, and to recover the desired model parameter posterior distributions in Eq. 6, we couple a forward model for multiple mineral phase age spectra and cumulative release curves as outlined in Section 2.1 with stochastic sampling via a Markov Chain Monte Carlo (MCMC) method. MCMC's are used to map out and sample probability distribution functions by stochastically exploring parameter space in such a way that a histogram of the samples produces the target prior distribution. For model parameters with priors that do not have a gradient (e.g., parameter(s) described by a uniform distribution), we couple a Metropolis and No U-Turn sampler (NUTS; Hoffman and Gelman, 2014), which we describe in more detail below. We use the NUTS sampler for all other

parameters in the model. The NUTS sampler was developed by Hoffman and Gelman (2014) as an extended form of the Hamiltonian Monte Carlo (HMC) formulated by Duane et al. (1987). Like all MCMC methods, HMC samplers are rooted in the Metropolis-Hastings algorithm, which follows the following procedure: (1) start with an initial, random model, (2) propose a new model, (3) compute the acceptance probability α of the proposed model, (4) assess if the model should be accepted by random comparison, and (5) repeat for a duration depending on the complexity of the model, typically at least ~10^5 iterations (Metropolis et al., 1953; Hastings, 1971). The acceptance criteria in our Metropolis Hastings algorithm is expressed as follows (after Gallagher et al., 2009):

$$\alpha = min\, pk'\, pyk'\, q(k|k')\, pk\, pyk\, q(k'|k) \quad (12)$$

where *k* is the current model and *k'* is the proposed model. The first two terms in the numerator and denominator of Eq. 12 are the prior and likelihood of the proposed and current models, respectively. The last term in both the numerator and denominator (q(*k*|*k'*)) is the proposal function, used to propose a new model vector *k'*, given the current model state *k*. Unlike the random walk nature of the Metropolis-Hastings sampler with the acceptance criteria for each proposal as defined in equation 12, NUTS takes advantage of first-order gradient information of the likelihood. In the model we use compound steps, meaning we use a combination of the NUTS and Metropolis samplers for our model depending on the distribution we have chosen for our parameters. We implemented our compound samplers in the probabilistic python library pymc3 (Salvatier et al., 2016). Code used to generate the models discussed here are available in a Github repository (https://github.com/jackcarter9/Bayesian-multi-component-40Ar-39Ar-dating).

3. RESULTS

3.1 Case study 1: VanLaningham and Mark (2011)

As a first test for our Bayesian modeling framework, we re-examine the $^{40}Ar/^{39}Ar$ age spectra generated by VanLaningham and Mark (2011). We chose these mixtures because they consist of neutron fluence monitors of known age and chemistry and individually exhibit a simple $^{40}Ar/^{39}Ar$ age spectrum (i.e., define an age plateau). Additionally, VanLaningham and Mark (2011) conducted their experiments using a temperature-controlled furnace, which enables us to

investigate diffusion kinetic parameters from their results. We only assume to know the number and composition of components in the mixture in our prior information.

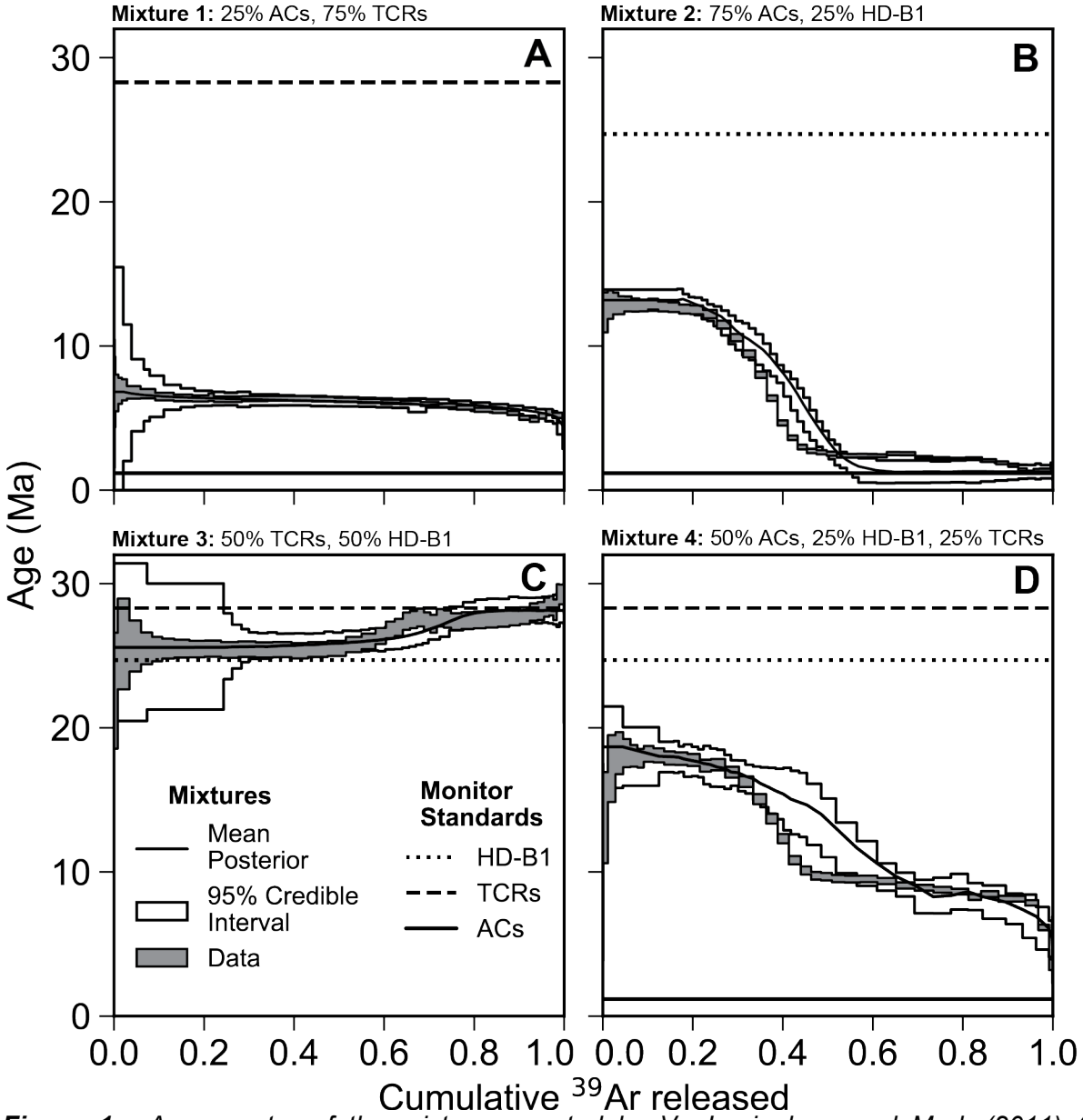

Figure 1. *Age spectra of the mixtures created by VanLaningham and Mark (2011) (gray boxes), the mean posterior predictive model of our Bayesian inversion (black solid curve), and the 95% credible interval of the posterior model (white boxes). The ages of neutron flux monitor standards used in these mixtures are indicated by horizontal lines and include Alder Creek sanidine (ACs, solid line), Heidelberg biotite (HD-B1, dotted line), and Taylor Creek Rhyolite sanidine (TCRs, dashed line). Known proportions of the monitor standards by mass in each mixture are indicated above each panel.*

Figure 1 shows the step heating results for the four mixtures originally presented in VanLaningham and Mark (2011). As an example, we focus on Mixture 2 (Figure 1B), comprised

of 75% ACs and 25% HD-B1 by mass. From Figure 1B, we observe that Ar release from the older HD-B1 is greater during the early low-temperature heating steps, which is due to a combination of the argon diffusion kinetics in these two mineral phases and the larger grain size of ACs relative to HD-B1 in this mixture. As the Ar from HD-B1 is exhausted, Ar release from the younger ACs becomes dominant in the high temperature steps. The exhaustion of Ar from HD-B1 results in monotonically-decreasing step ages from a 'pseudo plateau' at ~12 Ma corresponding to 0-25% of the cumulative ^{39}Ar released to another 'pseudo plateau' at ~2.2 Ma corresponding to 50-90% of the cumulative ^{39}Ar release. It is important to note that neither of these 'pseudo plateaus' corresponds to the known age of either ACs (1.19 ± 0.014 Ma (2σ analytical uncertainty) Vanlaningham and Mark, 2011; solid horizontal line, Figure 1B) or HD-B1 (24.59 ± 0.24 Ma (2σ analytical uncertainty), Vanlaningham and Mark, 2011; dotted horizontal line, Figure 1B). Note for comparison we used the ages for the fluence monitors as reported by Vanlaningham and Mark (2011) from their analyses of the individual age components. The ages of the individual components were calculated using the decay constants of Steiger and Jaeger (1977) and the age (28.02 Ma) of Fish Canyon Tuff sanidine (Morgan et al., 2014) as reported by Renne et al. (1998). For the purpose of our comparison the absolute age of the mineral standards is irrelevant (e.g., Mark et al., 2017).

While Figure 1 demonstrates that the shape of the age spectra for these mixtures depends on the ages of the components in the mixture, what is not immediately apparent in Figure 1 is the role of Ar diffusion kinetics in these components. In Figure 2, we show an Arrhenius plot calculated for Mixture 2, with the log of effective diffusivity, ln($Deffa2$), shown as a function of inverse temperature. Figure S1 also shows Arrhenius plots for Mixtures 1, 3, and 4. We calculated the effective Ar diffusion coefficients normalized for grain size (D_{eff}/a^2) using the fraction of ^{39}Ar released from each step in the degassing experiment after the equations in Fechtig and Kalbitzer (1966). We refer to an effective diffusion coefficient because each component of the mixture has a different diffusivity at each temperature in the degassing experiment. Therefore, we expect the calculated diffusivity for a particular temperature step to be a linear combination of the diffusivity in each phase *i*, weighted by their relative contributions f_i (Smith and Kay, 1999):

$$Deffa2 = i=1nfiDa2 \quad (13)$$

The Arrhenius behaviour we observe for Mixture 2 (Figure 2) is curvilinear and plots between argon diffusion parameters reported in the literature for sanidine (e.g., Cassata and Renne, 2013) and biotite (e.g., Harrison et al., 1985), the two mineral phases present in this mixture. This is consistent with our expectation that the effective diffusivity is a linear combination of the end-member diffusivities of each phase in the mixture (Eq. 13). At low temperatures and gas release fractions, we expect Ar diffusion from biotite to dominate and for diffusivities calculated for Mixture 2 to have a slope similar to the slope for biotite reported by Harrison et al. (1985). However, we note that temperatures of the furnace used to conduct the experiments by VanLaningham and Mark (2011) are not well-calibrated below ~800 ºC. Therefore, we suspect that temperatures < 800 ºC in Fig. 2 are poorly constrained, and that this results in a much steeper slope than expected from the kinetics reported by Harrison et al. (1985). We hypothesize that the temperature calibration also affects some of our model predictions (see Discussion section). At high temperatures and high gas release fractions, Ar from biotite becomes exhausted, and the diffusivities we calculate approach those expected for sanidine (Cassata and Renne, 2013).

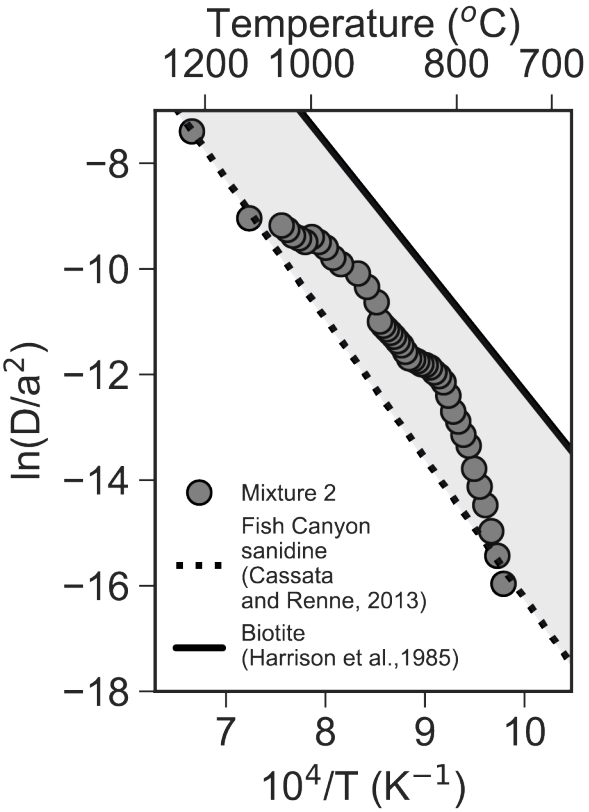

Figure 2. *Arrhenius plot for Mixture 2 (75% ACs and 25% HD-B1 by mass), calculated after Fechtig and Kalbitzer (1966). We compare the Arrhenius behavior of this mixture to kinetic*

parameters determined from step degassing experiments on Fish Canyon sanidine (dashed line; experiment FCs-1, Cassata and Renne, 2013) and biotite (solid line; Harrison et al., 1985). As Mixture 2 was sieved to a 20-63 um size fraction, we normalised the sanidine diffusivities by a diffusion length scale (i.e., grain half-diameter) of a = 32 μm and the biotite diffusivities to a = 10 μm, assuming a spherical geometry for both. This provides endmember constraints for comparison with the mixture's Arrhenius behavior, as a larger diffusion length scale for biotite would shift diffusivities down and vice versa for a smaller sanidine diffusion length scale. The effective Ar diffusivities calculated for Mixture 2 plot between the two end member diffusivities for sanidine and biotite.

Having demonstrated that the endmember diffusion kinetics are consistent with the mixture results, we use the endmember kinetics to inform the priors in our Bayesian inversion. Figure 3 shows the prior distributions for the variables that are utilized in our inversion for Mixture 2. We assume there are two components in the mixture *a priori* and that the mixture is compositional in nature. Therefore, the mixing coefficients of both components follow a Dirichlet distribution (Diebolt and Robert, 1994) (Figure 3A). We note that this is the fraction of ^{39}Ar contributed by each component, which is related but not equal to the mass of material from each component in the mixture. Figures 3B and C show the prior diffusion kinetics parameters we define using published experiments by Cassata and Renne (2013) and Harrison et al. (1985). In order to fully sample the kinetics parameters, we use the reported values from these experiments to construct distributions of the activation energies (E_a) (Figure 3B) and the natural logarithm of frequency factors ($\ln(D_0)$) (Figure 3C), treating the reported 2σ value as 1σ in the prior distribution. Figure 3D shows the prior age distribution for each component. To be as unrestrictive as possible, we define the prior age distribution as a uniform distribution with a lower bound of 0 and an upper age bound given by the age of the Earth.

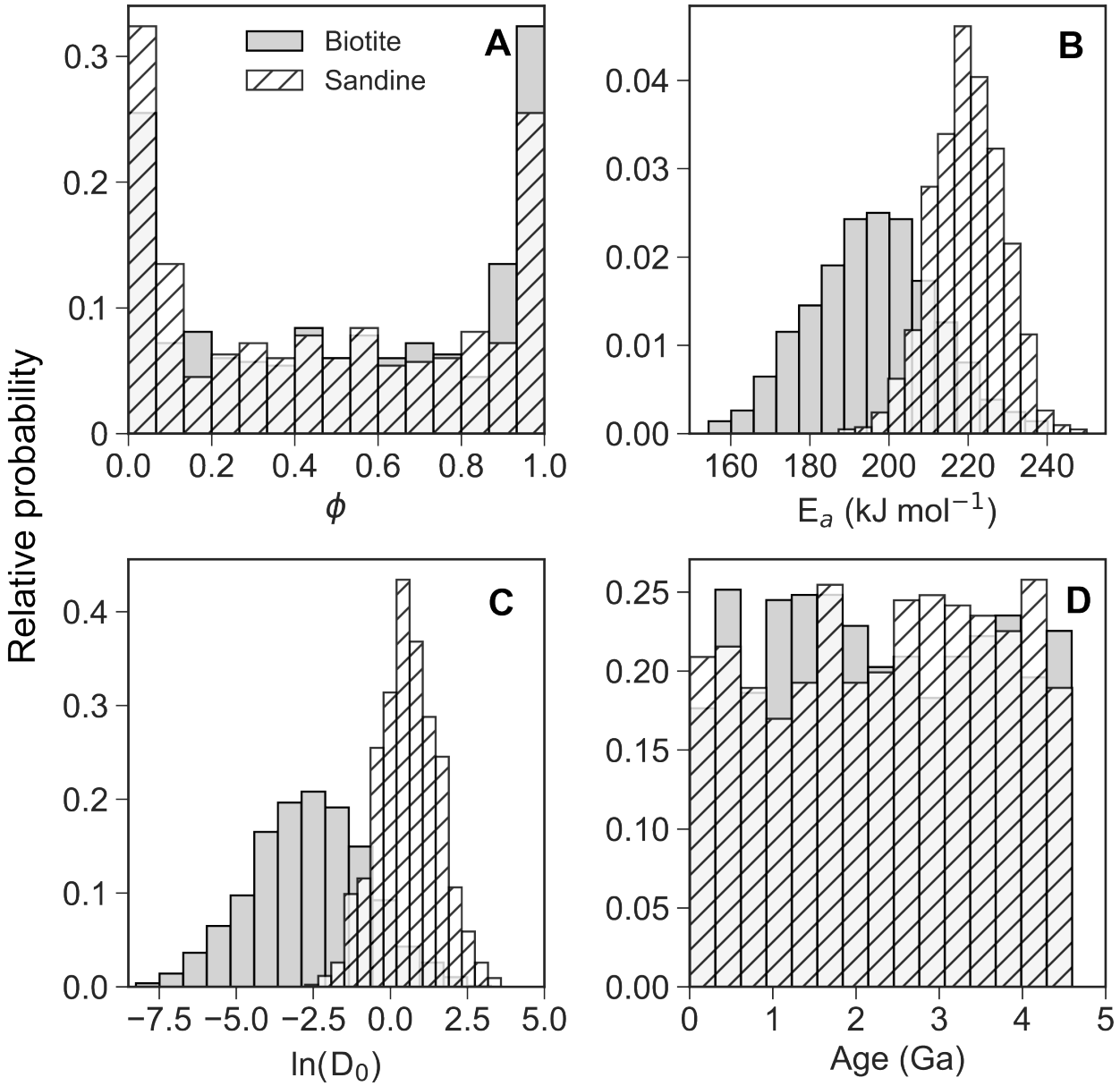

Figure 3. *Prior information used in our Bayesian deconvolution of Mixture 2, shown as relative probabilities. We assume to know the number (n = 2) and composition (biotite, shown in gray, and sanidine, shown in white stripes) of the components in the mixture. (**A**) Prior distribution of mixture fractions ϕ, assuming a Dirichlet boundary condition. (**B** and **C**) Prior distribution of activation energies (E_a) and the natural logarithm of frequency factors (ln(D_0), with D_0 normalised to 1 cm^{2}s^{-1}), estimated from the diffusion kinetics reported in Cassata and Renne (2013) and Harrison et al. (1985). (**D**) Prior distribution of component ages.*

Given these priors, we then ran our MCMC sampler 300,000 times, each time predicting the age spectrum and cumulative ^{39}Ar release curve. We assess the goodness of fit for each model result by comparing the model to the observations, which include both the age spectrum and cumulative ^{39}Ar release curve, via our likelihood function. Good fits, which minimize the summed

likelihood functions, suggests that the model, and therefore the parameters that build the model, may adequately describe the observation. The mean posterior model was then constructed from the model samples after the 'burn-in', which refers to the initial model samples that occur while the Markov chain explores parameter space widely before it reaches its equilibrium distribution. The mean posterior model from this post-burn-in sampling can then be compared directly with our observations. Figure 1 shows the mean posterior predictive models, also known as the expected models, from our Bayesian inversion of all four VanLaningham and Mark (2011) age spectra (solid black lines) and corresponding 95% credible intervals (white boxes, black outline). The expected models largely reproduce the complex age spectra observed in the laboratory experiments. The most significant differences typically occur during transition steps between 'pseudo' plateaus; nonetheless, most of these steps agree with the expected model within the credible interval, with the exception of Mixtures 2 and 4, wherein some steps during the transition are outside the model credible interval (Figures 1B and 1D). In Figure 4, we show the expected model for cumulative ^{39}Ar release for Mixture 2 compared to the observed cumulative ^{39}Ar release curve. We provide expected models of cumulative ^{39}Ar release curves for all four Vanlaningham and Mark (2011) mixtures in Figure S2. Our fits to the cumulative ^{39}Ar release curves are generally poorer than our fits to ^{40}Ar/^{39}Ar age spectra. For each cumulative release curve model fit, we see deviations from the observed ^{39}Ar release curve for the initial portion of the curve at lower temperatures.

In addition to reproducing the mixtures' cumulative ^{39}Ar release curves and age spectra, our aim was to deconvolve the age of each component in a mixture by sampling for these desired parameters from the posterior. Figure 5 shows the MCMC samples, after the initial burn-in period of 200,000 iterations, for the age of each component in Mixture 2. Figure 5 demonstrates that after the burn-in period, our model converges on ages for the two components in the mixture that minimize the log likelihood function (Figure 5C). Figure 6 shows a pair plot of the posterior sampling of component ages and diffusion kinetics for Mixture 2, where diagonal plots show histograms of a single parameter and off-diagonal plots show the correlations between parameters. Pair plots for the rest of the Vanlaningham and Mark (2011) mixtures are shown in Figures S3-S5.

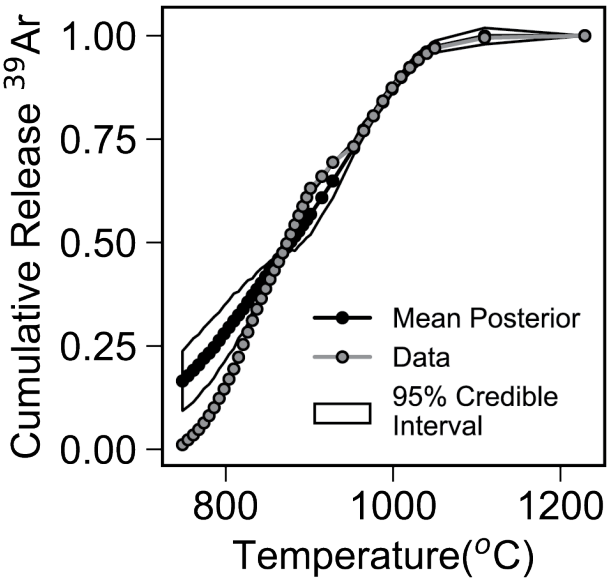

Figure 4. *Comparison of the observed (grey) and predicted (black with 95% credible interval) cumulative argon release curve for Mixture 2 (25% HD-B1, 75% ACs), of Vanlaningham and Mark (2011).*

499

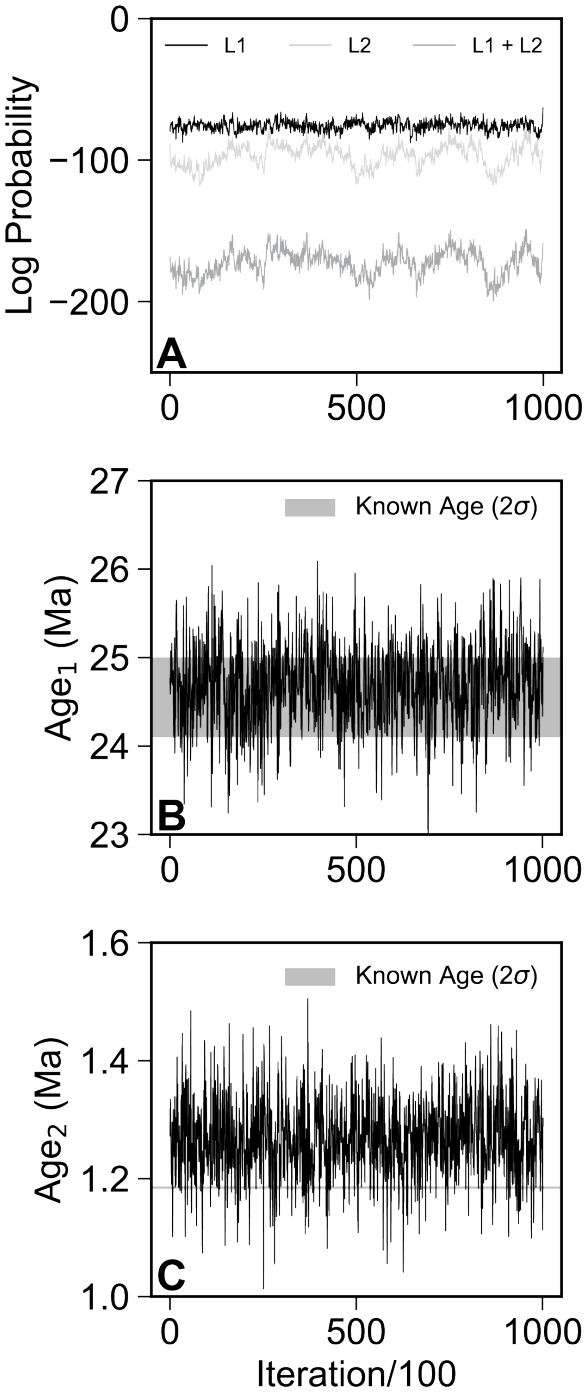

Figure 5. (A) *Log likelihood of each model age spectrum (L1) and cumulative release curve (L2), as well as the summed log likelihood (L1 + L2), for Mixture 2 of Vanlaningham and Mark (2011). Note that the summed log likelihood and L1 plot on top of one another. (**B**) and (**C**) are accepted sample ages of HD-B1 and ACs in the mixture created by Vanlaningham and Mark (2011). Every 100th accepted sample for the post-burn-in iterations is shown. For reference, the known age of HD-B1 (**B**) and ACs (**C**) are shown at the 95% confidence interval with grey horizontal bars.*

500

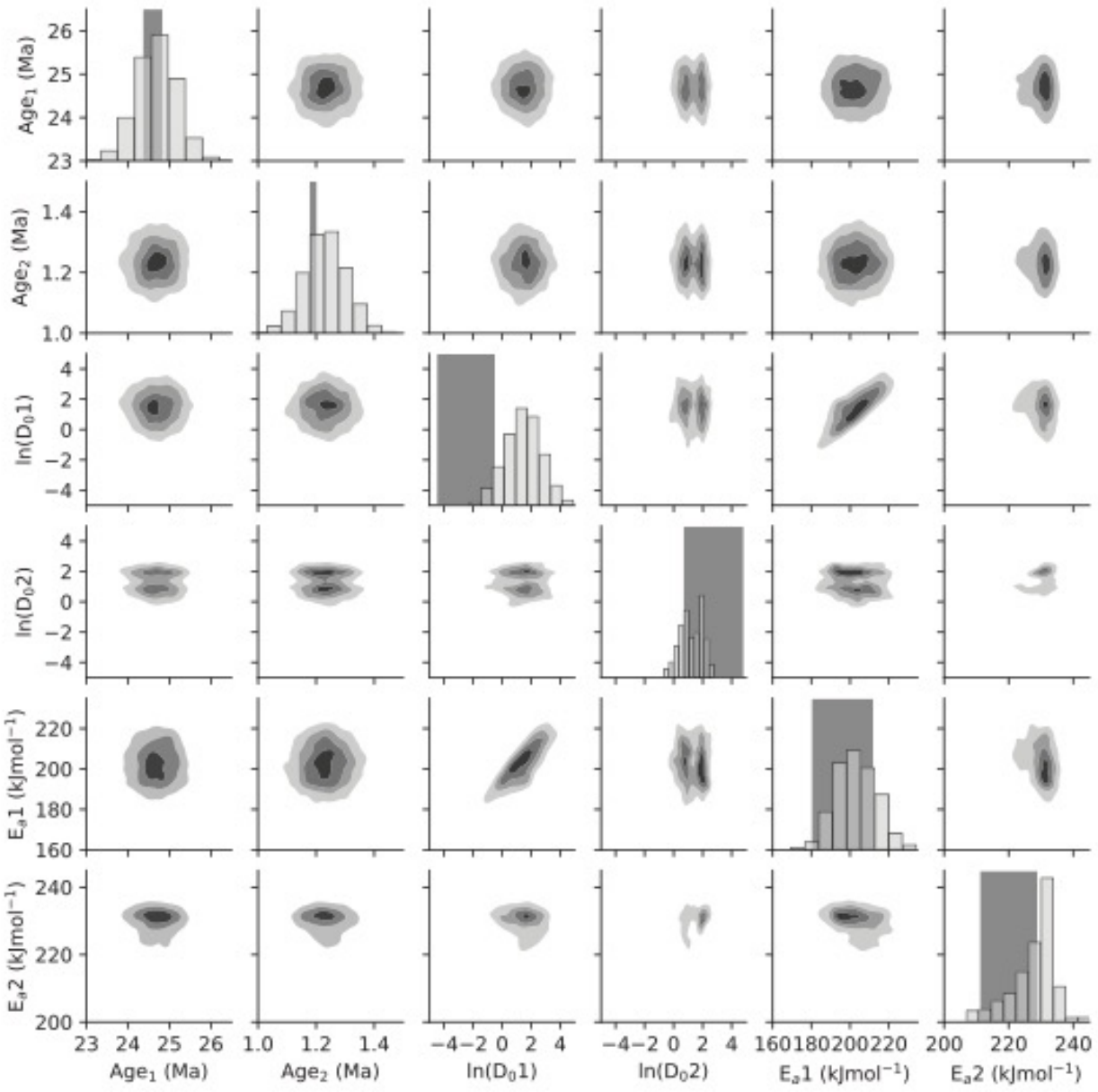

***Figure 6**. Pair plot for Vanlaningham and Mark (2011) Mixture 2 showing the posterior sampling of each component's age (Ma), activation energy (Ea, kJ/mol) and the natural logarithm of frequency factors (ln(D_0), with D_0 normalised to 1 cm^2s^{-1}). In diagonal histogram plots, dark grey boxes represent the 95% confidence bounds of the known parameter values from prior studies (Harrison et al., 1985; Vanlaningham and Mark, 2011; Cassata and Renne, 2013;). We interpret component 1 to be HD-B1 (accepted age of 24.59± 0.24 Ma; Vanlaningham and Mark, 2011) and component 2 as ACs (accepted age of 1.19 ± 0.014 Ma; Vanlaningham and Mark, 2011). In the off-diagonal kernel density estimation plots, four contours are shown from light to dark gray representing 95, 68, 34 and 5% credible intervals.*

501

502

503

Table 1. *Deconvolution model results for the VanLaningham and Mark (2011) mixtures, compared to known ages for mixture components.*

Component	Accepted Age ± 2σ (Ma)	Estimated Age ± 2σ (Ma)
Mixture 1 : 75% Alder Creek sanidine (ACs), 25% Taylor Creek Rhyolite sanidine (TCRs)		
ACs	1.19 ± 0.014[1]	1.21 ± 0.15
TCRs	28.26 ± 0.28[1]	28.0 ± 1.0
MIxture 2: 75% ACs, 25% Heidelberg biotite (HD-B1)		
ACs	1.19 ± 0.014[1]	1.27 ± 0.16
HD-B1	24.59 ± 0.24 [1]	24.6 ± 1.1
Mixture 3: 50% HD-B1, 50% TCRs		
HD-B1	24.59 ± 0.24[1]	24.8 ± 0.8
TCRs	28.26 ± 0.28[1]	28.1 ± 0.6
Mixture 4: 50% ACs, 25% HD-B1, 25% HD-B1		
ACs	1.19 ± 0.014	1.20 ± 0.12
TCRs	28.26 ± 0.28	28.0 ± 1.0
HD-B1	24.59 ± 0.24	25.0 ± 1.0

[1] VanLaningham and Mark (2011)

Overall, we found that our Bayesian inversion method successfully modeled the ages and diffusion kinetics for each component in the VanLaningham and Mark (2011) mixtures. This is illustrated in Figure 6 for Mixture 2 (on-diagonal histograms), as well as for all four mixtures in Table 1 and Figures S3-S5. The ages of the components we estimate from the posterior sampling are statistically indistinguishable from the known ages of the components in each mixture (Table 1), although the age uncertainty from the posterior estimate is greater than the uncertainty of the known age. We do not observe any significant differences in the relative uncertainty of model-predicted ages as a function of the number of components, nor do we observe any significant differences in predicted age uncertainty as a function of which phases are present in a mixture. We find that the relative uncertainty in the predicted age for Alder Creek sanidine (ACs), which is by far the youngest component with an age of 1.19 ± 0.014 Ma (Vanlaningham and Mark, 2011), is greater (by a factor of x3-6) than the relative age uncertainty for the other three, older monitor standards. We also find that, although indistinguishable within the uncertainties reported, our estimated ages for ACs are nominally older than the known age; likewise, our estimated ages for the oldest components in a given mixture (either HD-B1 or TCRs) are nominally younger than the known age. We explore possible reasons for these differences in our discussion section.

3.2 Case study 2: Kula et al (2010)

In the first case study, specifically Mixtures 1 and 4, we examined mixtures containing components of the same mineral, but did not observe this to have a clear effect on the model predicted ages or their relative uncertainties. Here, we reevaluate the muscovite and biotite mixture data presented by Kula et al. (2010) as an endmember, limiting case of mixtures with multiple components of the same mineral. Our expectation is that this scenario should be challenging for our simple Bayesian model, since the individual components will have very similar and possibly identical argon diffusion kinetics. In their study, Kula et al. (2010) created mixtures of two muscovite and biotite samples, respectively, that individually yield robust age plateaus (97-100% of the ^{39}Ar release). The individual muscovite components yielded ^{40}Ar/^{39}Ar plateau ages as follows: IV14, with an age of 148.8 ± 1.6 Ma (2σ), and NY25, with an age of 71.9 ± 0.8 Ma (2σ). Similarly, the individual biotite components yielded ^{40}Ar/^{39}Ar plateau ages as follows; IV8, with an age of 146.1 ± 1.6 Ma (2σ), and PM1, with an age of 75.3 ± 0.8 Ma (2σ). Kula et al. (2010) created three mixtures with different ratios of the muscovite or biotite samples by mass (3:1, 1:1, and 1:3 IV14 to NY25 and IV8 to PM1). The ^{40}Ar/^{39}Ar age spectra and cumulative ^{39}Ar release curves from incremental heating of these muscovite and biotite mixtures are reproduced in Figures 7 and 8, respectively. The muscovite mixtures show similar features to Mixture 1 of VanLaningham and Mark (2011) in that, to a first order, they observe similar ages for most steps that are proportional to the mixing fractions (Kula et al., 2010). The biotite mixtures show highly discordant spectra with an overall decrease in age toward the younger PM1 component but with localised undulation of step ages.

We initially set up our Bayesian deconvolution model with priors analogous to those set up for case study 1. Specifically, we fixed the number of components in each mixture to 2, used the diffusion kinetics of argon in muscovite and biotite reported by Harrison et al. (2009) and Harrison et al. (1985) respectively, and allowed the component ages to be free parameters described by uniform distribution. We found that with these unrestrictive priors, our modeled step ages agree with essentially all of the steps in the observed age spectra, and generally have much larger credible intervals than the observed uncertainties in step ages (Figures S6-7, A-C). In the muscovite models, the mean posterior age spectra are flat for > 85% of the cumulative ^{39}Ar, whereas the observed age spectra exhibit an overall slight upward increase in age over this gas fraction, although these increases occur within the modeled 95% credible intervals (Figure S6 A-C). Over the last < 15% of the cumulative ^{39}Ar release, the predicted step ages decrease and approach the age of the final observed step age. In the case of the biotite mixtures, while the undulations in the observed age spectra are generally within our models'

very large credible intervals, our mean posterior age spectra exhibit monotonic decrease in step age with increasing ^{39}Ar release fraction that is notably different from the observed age spectra shapes. We also found differences between the predicted and observed cumulative ^{39}Ar release curves for these mixtures when using a model setup with unrestrictive priors (Figures S6-7, D-F). For the muscovite mixtures, we consistently predict higher ^{39}Ar release fractions at low temperatures than observed in experiments (Figure S6, D-F). Conversely, for two of the three biotite mixtures we predict lower ^{39}Ar release fractions at low temperatures than observed in experiments, although in this case the observed values are very close to the wide model credible interval (Figure S7, D-F).

While the predicted age spectra and cumulative ^{39}Ar release curves provide some insight about the model's performance with the unrestrictive prior, we are most interested to know about the model's ability to resolve the ages of different components present in the mixture. For the muscovite mixtures, our model technically resolves the presence of two components. However, in all cases our model predicts that one component completely dominates the mixture and fails to predict the age of either component in the mixtures, with the exception of the younger component in the 1:3 IV14:NY25 mixture (Table 2). For example, in the 3:1 IV14:NY25 mixture, the older component carries 99% of the mixture weight. The ~133 Ma modeled age of the older component is consistent with the apparent plateau age in the observed age spectrum (Figure S6A), but is inconsistent with the known age of IV14, the older component in this mixture, of ~149 Ma (Table 2). Similarly, the modeled age of the younger component is ~100 Ma, which is consistent with the youngest step ages observed at the end of the step heating experiment (Figure S6A) but inconsistent with the ~72 Ma age of NY25, the younger component in this mixture (Table 2). For the biotite mixtures, the mixing fractions predicted for the biotite mixtures with the unrestrictive prior are also inconsistent with the known mixing fractions, although we do resolve the presence of two components. For example, in the 1:3 IV8:PM1 mixture, our model predicts mixing fractions of 57% IV8 and 48% PM1. With the unrestrictive prior we predict component ages that either 1) correspond to the initial and final step ages of the observed age spectra (Figure S7 A-C), which do not correspond to either of the known ages of the individual components, or 2) have very large uncertainties, such that the ages of the individual components are indistinguishable (Table 3).

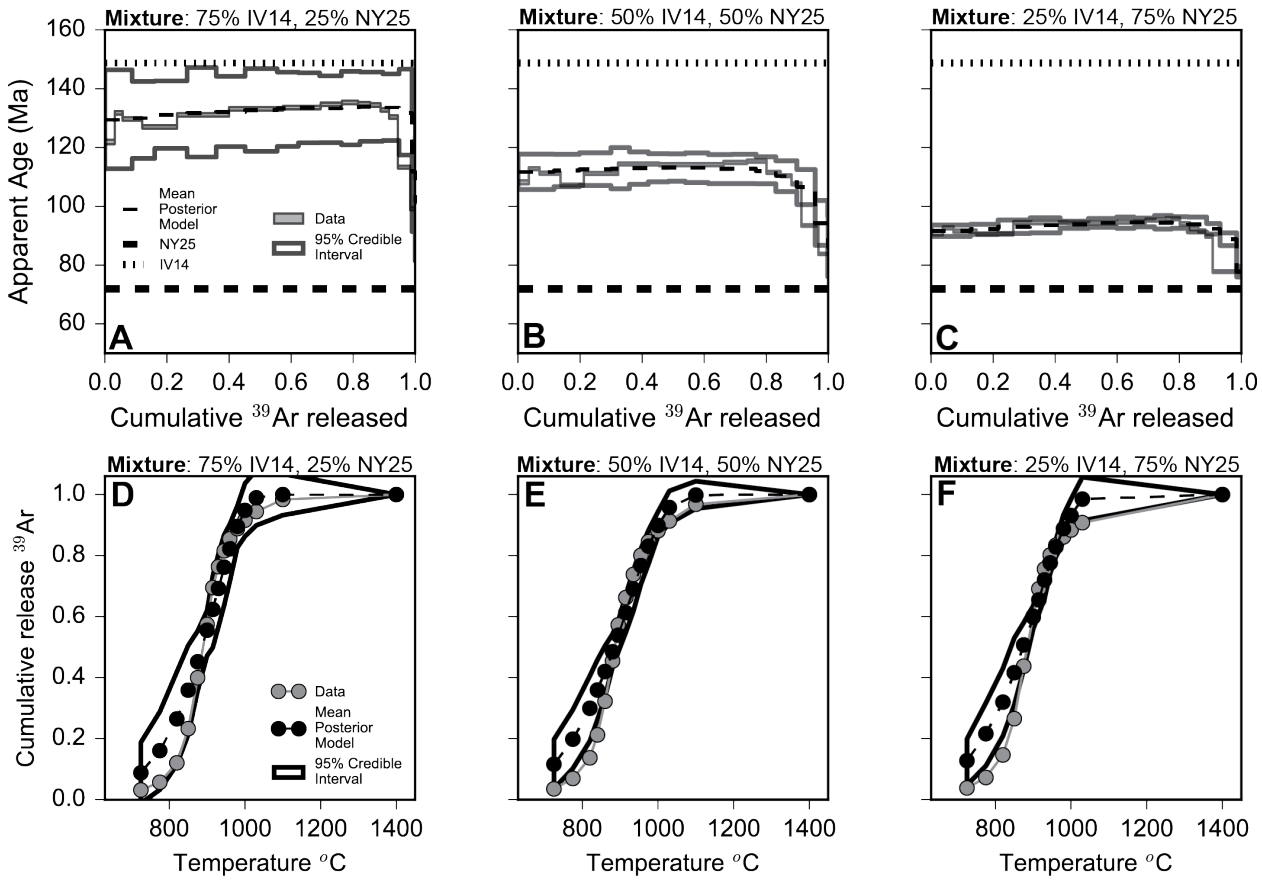

Figure 7. *Age spectra (**A, B, C**) and cumulative release curves (**D, E, F**) of muscovite mixtures created by Kula et al. (2010). Each mixture contains grains from two muscovite samples, mixed in different proportions by mass: IV14 (stippled line,* 148.8 ± 1.6 *Ma), and NY25 (dashed line,* 71.9 ± 0.8 *Ma). The observed age spectra and cumulative release curves are shown in grey. The mean posterior age and cumulative release models are given by a black dashed line, with the 95% credible interval is shown with a solid gray line. Models shown are for the more restrictive priors on the mixing fraction of each component described in the text.*

591

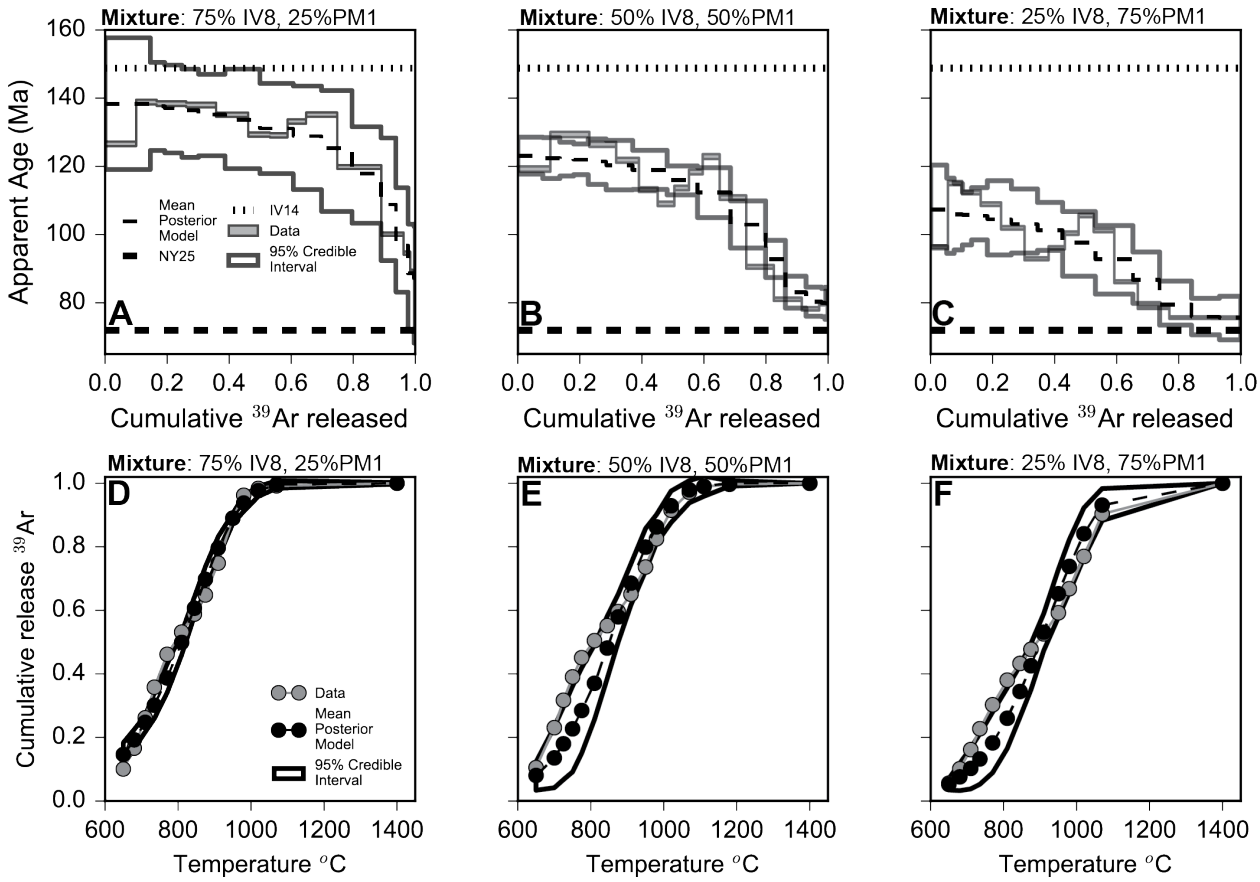

Figure 8*. Age spectra (**A, B, C**) and cumulative release curves (**D, E, F**) of biotite mixtures created by Kula et al. (2010). Each mixture contains grains from two biotite samples, mixed in different proportions by mass: IV8 (stippled line,* 146.1 ± 1.6 *Ma), and PM1 (dashed line,* 75.3 ± 0.8 *Ma). The observed age spectra and cumulative release curves are shown in grey. The mean posterior age and cumulative release models are given by a black dashed line, with the 95% credible interval is shown with a solid gray line. Models shown are for the more restrictive priors on the mixing fraction of each component described in the text.*

To attempt to successfully deconvolve the age components for Kula et al. (2010) mixtures, we imposed more restrictive priors. Specifically, we placed a tighter constraint on the prior for the mixture fraction of each component. For example, for a mixture with a known mixture fraction by mass of 1:3, we constrain one component to have a mixture fraction between 0.2 and 0.3 and the other to be between 0.7 and 0.8. Imposing this more restrictive prior ensures that there is a weight assigned to the fraction of each component that is within the known range of mixture weights for the prepared samples, which prevents the model from collapsing to a single component of intermediate age between the individual component ages, as we observed for the muscovite mixtures. Modeled component ages for both the initial model setup with unrestrictive priors and this setup with more restrictive mixture priors are given in Tables 2 and 3. We also

603 report model results with these more restrictive priors as pair plots of the diffusion kinetics and
604 ages of each component in the Kula et al. (2010) mixtures in Figures S8-13.
605
606 With a more restrictive prior on the mixing fractions, our model does a better job of reproducing
607 the complexities of the observed $^{40}Ar/^{39}Ar$ age spectra of the muscovite mixtures. Specifically,
608 our model predicts slightly increasing step ages by 80% or more of the ^{39}Ar release, followed by
609 decreasing step ages in the last ~20% or less of ^{39}Ar release (Figure 7 A–C). In contrast, our
610 model is unable predict the cumulative release curves for the muscovite mixtures; specifically,
611 our model predicts an earlier ^{39}Ar release than observed in the experiments over the initial 50%
612 of the ^{39}Ar release (Figure 7 D–F). We predict ages for the muscovite mixture components that,
613 in all but one case, are within the 2σ confidence limit of the known ages of NY25 and IV14. The
614 one case in which we do not predict the component age is for the younger component in the 3:1
615 IV14:NY25 mixture. The relative uncertainty of the component ages for these muscovite
616 mixtures are larger than the relative uncertainties we obtained for component ages in case
617 study 1.
618
619 Imposing a more restrictive prior for the biotite mixtures enabled us to predict component ages
620 that agree with the known component ages within the modeled credible interval for all three
621 mixtures. However, like the muscovite mixtures we predict a much larger relative uncertainty in
622 the estimated component ages than is observed for the individual biotite components (Table 3),
623 and also much larger relative uncertainties compared to the results in case study 1. The
624 posterior predicted age spectra for the biotite mixtures are similar to the overall observed age
625 spectra, in that step ages decrease with increasing cumulative ^{39}Ar, with a much higher age
626 gradient toward the end of the experiments. However, our modeled age spectra still lack the
627 complexity in the age spectra observed for these mixtures, particularly the two 'undulations'
628 observed over the first 60-80% of ^{39}Ar release. Unlike the muscovite mixtures, our modeled
629 cumulative release curves exhibit a later ^{39}Ar release than observed in the experiments for the
630 first 50% of the ^{39}Ar release.
631

Table 2*. Modeled ages, using both nonrestrictive and restrictive priors, for muscovite components in mixtures created by Kula et al. (2010), with comparison to known ages.*

	Accepted age ± 2σ (Ma)	Estimated age ± 2σ (Ma) unrestrictive prior	Estimated age ± 2σ (Ma) restrictive prior
Known: 3:1(IV14:NY25)			
IV14	148.8 ± 1.6	133 ± 7	143 ± 5
NY25	71.9 ± 0.8	100 ± 10	100 ± 8

Known: 1:1(IV14:NY25)			
IV14	148.8 ± 1.6	114 ± 12	137± 21
NY25	71.9 ± 0.8	88 ± 15	87 ± 16
Known: 1:3(IV14:NY25)			
IV14	148.8 ± 1.6	94 ± 6	138 ± 26
NY25	71.9 ± 0.8	78 ± 8	78 ± 7

Table 3*. Modeled ages, using nonrestrictive and restrictive priors, for biotite components in mixtures created by Kula et al. (2010), with comparison to known ages and mixing fractions.*

	Accepted age ± 2σ (Ma)	Estimated age ± 2σ (Ma), unrestrictive prior	Estimated age ± 2σ (Ma), restrictive prior
Known: 3:1(IV8:PM1)			
IV8	146.1 ± 1.6	130 ± 4	149 ± 14
PM1	75.3 ± 0.8	128 ± 5	85 ± 13
Known: 1:1(IV8:PM1)			
IV8	146.1 ± 1.6	129 ± 38	141 ± 34
PM1	75.3 ± 0.8	80 ± 6	80 ± 5
Known: 1:3(IV8:PM1)			
IV8	146.1 ± 1.6	158 ± 78	152 ± 25
PM1	75.3 ± 0.8	65 ± 32	76 ± 3

3.3 Case study 3: A hypothetical *in-situ* Martian experiment

While we use the previous two case studies to investigate the strengths and weaknesses of our Bayesian approach, it is also insightful to demonstrate our Bayesian framework for a geologically interesting case study. For this purpose, we created a hypothetical $^{40}Ar/^{39}Ar$ dataset for the Martian surface using compositional data from previous Mars rover observations. The recent successes of rover-based missions to Mars, such as the Mars Science Laboratory (MSL) and Mars Exploration Rover (MER) missions, have pushed the development of an *in situ* absolute dating package for future rover-based missions (Swindle et al., 2003; Anderson et al., 2012, Cassata, 2014; Cohen et al., 2014; Solé, 2014; Cho et al., 2017; Morgan et al., 2017). The ubiquity and dominance of primary K-bearing silicate minerals (e.g., Ehlmann and Edwards, 2014), makes the K–Ar system one of the most promising radioisotopic systems for dating materials *in situ* on the surface of Mars.

All existing *in situ* K-Ar ages from Mars, obtained by the Curiosity rover in Gale Crater, are from multi-component mixtures of K-bearing minerals (Farley et al., 2014; Vasconcelos et al., 2016; Martin et al., 2017). Interpreting these analyses requires a number of assumptions about the ages and distribution of K and Ar in individual components in the mixture. Assumptions about the distribution of Ar could potentially be addressed by putting a ^{251}Cf source on future rovers,

652 which would be used to irradiate samples with neutrons and allow for *in situ* $^{40}Ar/^{39}Ar$ rather than
653 K-Ar (Morgan et al., 2017). Nonetheless, *in situ* measurements on future missions will still very
654 likely be applied to mineral mixtures, as mineral separation capabilities on rovers are currently
655 limited to simple processes such as simple sieving (e.g., Mahaffy et al., 2012; Farley et al.,
656 2014). Our Bayesian approach could therefore be important for interpreting future $^{40}Ar/^{39}Ar$
657 datasets from *in situ* measurements on mixtures, and also for $^{40}Ar/^{39}Ar$ studies in future sample
658 return missions (e.g., Williford et al., 2018) where the amount of material is too small or the risk
659 of losing material too great to carry out mineral separations.
660
661 We generated a hypothetical $^{40}Ar/^{39}Ar$ dataset based on existing mineralogical and age
662 information from the Murray mudstone Formation explored by the Curiosity rover. Of the mineral
663 phases detected in the Murray Formation, jarosite, plagioclase, and sanidine contain sufficient K
664 to contribute argon to an $^{40}Ar/^{39}Ar$ age spectrum (Rampe et al., 2017). A large amorphous
665 fraction detected in the Murray Formation may also contain phases with nontrivial K
666 abundances; however, because the exact composition and therefore diffusion kinetics of any K-
667 bearing phase are not known, we ignore this component at present (Rampe et al., 2017). Martin
668 et al. (2017) carried out a two-step K-Ar dating experiment at the Mojave 2 site in the Murray
669 Formation. The first step at 500 ºC yielded an age of 2.12 ± 0.72 Ga (2σ), which Martin et al.
670 (2017) associate with low retentivity jarosite and possibly K-bearing salts present in the
671 amorphous fraction. They attribute this relatively young age for secondary mineralization to the
672 presence of fluids on the Martian surface at or slightly before this date. The second step at 930
673 ºC yielded an age of 4.07 ± 1.36 Ga (2σ), which the authors ascribe to a detrital component of
674 plagioclase, similar to the results obtained for bulk degassing of material in the Sheepbed
675 mudstone (4.21 ± 0.71 Ga 2σ; Farley et al., 2014).
676
677 For our hypothetical mixture, we use the mineral composition measured at Telegraph Peak
678 (Figure 8A; Rampe et al., 2017) rather than the Mojave 2 site, as the latter lacks sanidine. We
679 treat sanidine and plagioclase as separate components and assume both are Noachian in age,
680 consistent with the existing *in situ* chronology (Farley et al., 2014; Martin et al., 2017), but give
681 these two components slightly different ages (4.10 ± 0.05 and 4.30 ± 0.2 Ga (2σ) for sanidine
682 and plagioclase, respectively) in order to test whether our Bayesian approach can resolve the
683 age difference. We ascribe an age of 2.10 ± 0.25 Ga (2σ) to a jarosite component after the low-
684 temperature degassing age obtained by Martin et al. (2017). Given these ages and
685 compositions of components, we calculated an age spectrum for the synthetic mixture (Figure

9B) assuming diffusion kinetics for the mineral phases present that are reported in the literature (Kula and Baldwin, 2011; Cassata and Renne, 2013; Jourdan and Eroglu, 2017) and a grain size of 100 μm for each component (chosen as CheMin drill samples are typically < 150 μm, Rampe et al., 2017).

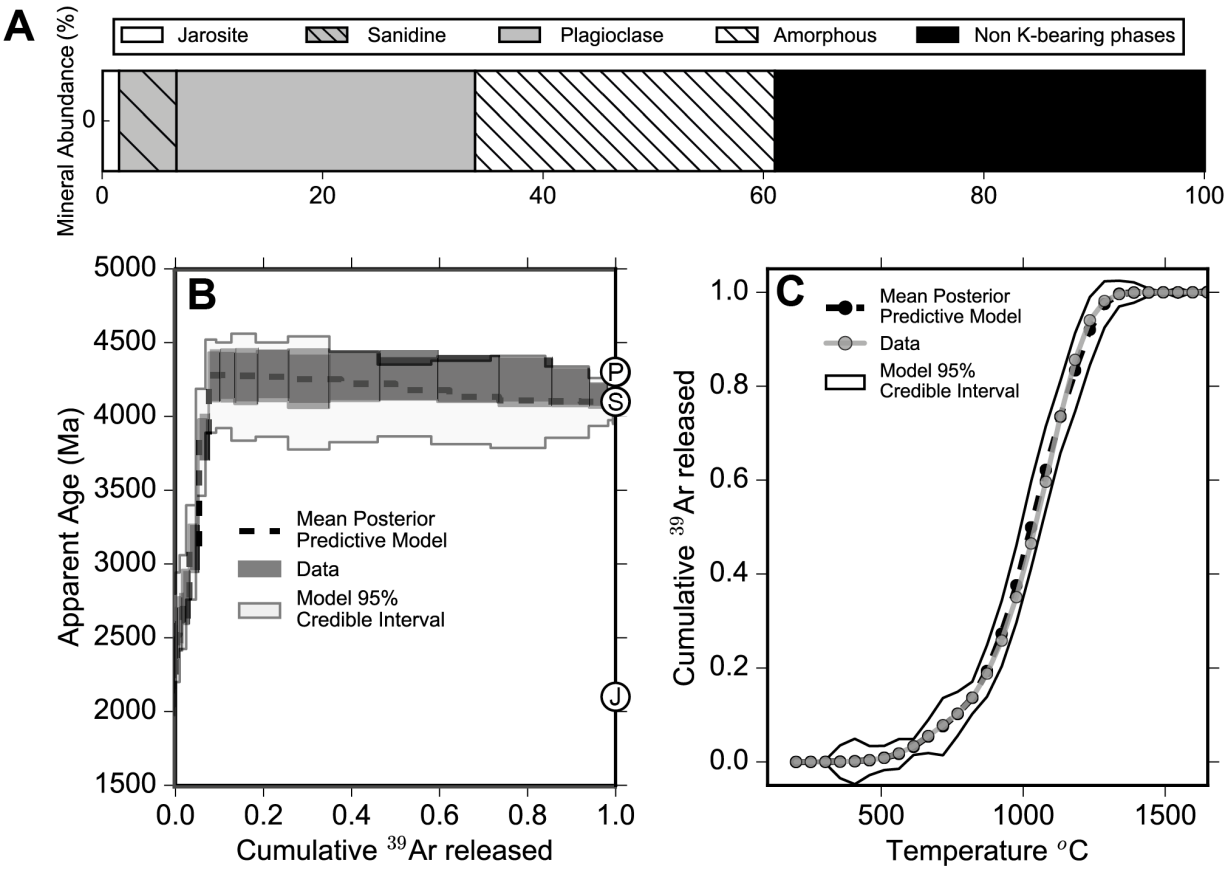

Figure 9. *(**A**) Mineral abundances in weight % of the Murray mudstone formation measured by CheMin at Telegraph Peak, after Rampe et al. (2017). We use the relative abundances of K-bearing phases shown (jarosite, sanidine, and plagioclase), previously-determined in situ K-Ar ages (Martin et al. 2017), and published diffusion kinetics to generate (**B**) a hypothetical $^{40}Ar/^{39}Ar$ age spectrum for a bulk sediment analysis at this site and (**C**) a hypothetical cumulative ^{39}Ar release curve. Mean posterior models (dashed black lines) for both the age spectrum and cumulative ^{39}Ar release curve are shown in **B** and **C.** Input ages for the plagioclase P, sanidine S, and jarosite J components are shown with circles on the right-hand side of **B**.*

Table 4. *Estimated ages for the synthetic Martian regolith mixture.*

Component	Input Age ± 2σ (Ga)	Estimated Age ± 2σ (Ga)
Jarosite	2.10 ± 0.25	2.2 ± 0.2
Sanidine	4.10 ± 0.05	4.11 ± 0.04
Plagioclase	4.3 ± 0.2	4.4 ± 0.3

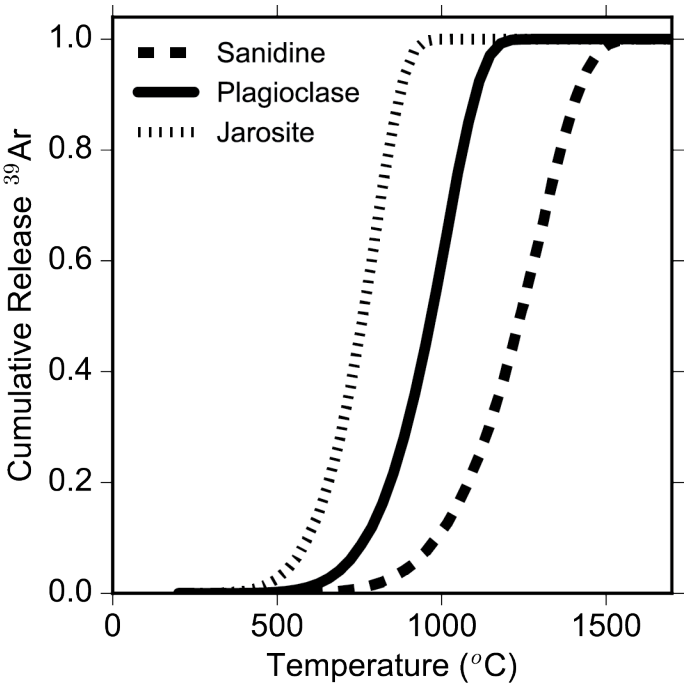

Figure 10. *Individual cumulative release curves for the three K-bearing components in our synthetic Martian regolith dataset: jarosite, plagioclase, and sanidine. Calculations were carried out using the discretized solution of fractional loss for a sphere by Fechtig and Kalbitzer (1966) and using diffusion kinetics taken from literature studies on each of the components in the mixture (Cassata et al., 2009; Cassata and Renne, 2013; Kula and Baldwin, 2011). The kinetics used in our model are scaled to a grain size of 100 μm.*

The synthetic age spectrum we generated (Figure 9B) shows patterns similar to that expected from a sample that has undergone diffusive argon loss, which manifests as monotonically increasing step ages with increasing cumulative ^{39}Ar release in the early part of the step degassing experiment. Unlike a case of thermally driven loss, our monotonically increasing step ages in the early to middle part of the experiment are due to the competing degassing of both jarosite, the youngest and least retentive component, and the oldest and intermediately retentive component plagioclase. To demonstrate this, Figure 10 shows the cumulative ^{39}Ar release curves for the three mineral phases in this hypothetical mixture using the same diffusion kinetics as used to generate the age spectrum. Figure S14 also shows the incremental ^{39}Ar release curve for each component, as well as the incremental and cumulative ^{39}Ar release curves for the hypothetical mixture. We can see in Figure 10 that, by 800 ºC, near complete degassing of jarosite has occurred, while only ~20% and < 5% of ^{39}Ar has degassed from plagioclase and sanidine, respectively. In the latter stages of release, both plagioclase and sanidine degas in concert, with plagioclase exhausting first (Figure 10), resulting in the small

stepped decrease in age from the older plagioclase (4.3 Ga) to the younger sanidine (4.1 Ga) observed in our synthetic age spectrum.

In our synthetic Martian dataset we assume diffusion kinetics priors from previous studies on the end-member K-bearing components (Cassata et al., 2009; Cassata and Renne, 2013; Kula and Baldwin, 2011) and assumed a variance of 2σ for these values as in our other case studies. We also assume a Dirichlet prior for the mixing fractions with no constraints for any component, and set the prior for all age components to be a uniform distribution between 0 and 4.6 Ga to encompass the age of the Solar System.

Following our creation of this synthetic Martian regolith $^{40}Ar/^{39}Ar$ dataset we simultaneously invert both the fractional release curve and age spectrum with our Bayesian model. We report the estimated ages of each end member component in table 3 and show mean posterior models and confidence intervals for the age spectrum and ^{39}Ar cumulative release curve in figure 9. A pair plot showing the relationship between the posterior estimates of ages and diffusion kinetics for all components in the mixture is given in supplementary figure S15. The posterior models of both the age spectrum and cumulative ^{39}Ar release curve agree with the data within the 95% credible interval. The probability density estimates of age components in the mixture, which we draw from the posterior model, agree with the known input ages and have relative uncertainties of ~1-7% (2σ).

4. DISCUSSION

The aims of the Bayesian method developed here are to: (1) fit a posterior predictive model to $^{40}Ar/^{39}Ar$ datasets from mixtures of multiple components, and (2) estimate the values of model parameters, principally the $^{40}Ar/^{39}Ar$ ages of each component in the mixture. Below, we discuss what factors influence the degree to which our Bayesian approach was successful in meeting these aims for each of our case studies. We then compare our approach to existing approaches for interpreting $^{40}Ar/^{39}Ar$ datasets from mineral mixtures and discuss ways in which our Bayesian model could be improved upon, to yield better component age estimates as well as deal with more complex $^{40}Ar/^{39}Ar$ datasets. Finally, we outline several applications where we foresee our Bayesian approach being useful for answering geologic questions.

4.1 Model fits and parameter estimation

742 *4.1.1 Case study 1*

743 Our first case study, using stepwise heating experiments of mixtures of neutron fluence
744 monitors created by Vanlaningham and Mark (2011), is in many ways ideally designed to meet
745 the assumptions set forth in our model framework. We know from previous work on the
746 individual components in these mixtures that each component loses argon by volume diffusion
747 and experienced geologically instantaneous cooling, therefore exhibiting no evidence for
748 diffusive loss of $^{40}Ar^{*}$. For TCRs and ACs, which consist of roughly equant grains, the
749 assumption of a spherical diffusion geometry is also well-justified. Although an infinite sheet
750 diffusion geometry may be more appropriate for HD-B1, this does not affect our model results in
751 a statistically significant way. For example, if we assume an infinite sheet geometry for HD-B1 in
752 Mixture 2, we obtain a similar fit to the age spectrum for early cumulative ^{39}Ar release fractions
753 (Figure S16) and results in a 1% difference in modeled age of HD-B1 and a 5% difference in the
754 modeled age of ACs (Fig S17). Importantly, both sets of modeled ages agree with the known
755 component ages within their credible intervals. With these assumptions of our model framework
756 about volume diffusion and geometry met, we find a good fit between our posterior models and
757 the observed $^{40}Ar/^{39}Ar$ age spectra, with most step ages agreeing within the 95% credible
758 interval of the expected model (Figure 1). This demonstrates that, when the assumptions of our
759 model framework are valid, we can use our Bayesian approach to meet our first goal of fitting a
760 posterior predictive model to $^{40}Ar/^{39}Ar$ datasets from mixtures of multiple components. This is
761 the case even with essentially uninformed priors about the mixing fractions and ages of
762 individual components (Figure 3).
763
764 Our fits to the cumulative ^{39}Ar release curves, shown in Figures 4 and S2, are generally poorer
765 than our fits to $^{40}Ar/^{39}Ar$ age spectra for this case study. For each cumulative release curve
766 model fit, we see deviations from the observed cumulative ^{39}Ar release at low release fractions
767 and low temperatures. The most likely explanation for this initial deviation in cumulative ^{39}Ar
768 release is the inaccurate calibration of the furnace used to heat the samples at temperatures
769 below ~800 ^{o}C. Specifically, we think the furnace temperature for heating steps below 800 ºC is
770 overestimated. Our comparison of the Vanlaningham and Mark (2011) apparent diffusivities to
771 known diffusion kinetics for the individual components these mixtures (Fig. 2, S1) supports this
772 hypothesis, as we observe much lower diffusivities and a greater rate of increase in diffusivity
773 than expected for the nominal temperatures below 800 ºC in these experiments. This is also
774 consistent with what we observe for the cumulative ^{39}Ar release curves, as our models
775 consistently predict higher initial ^{39}Ar losses than observed experimentally (Fig. 4, S2). The

776 nature of a cumulative quantity means that this overprediction of initial ^{39}Ar loss affects the
777 predicted cumulative ^{39}Ar loss at all subsequent temperature steps, which for some of the
778 cumulative ^{39}Ar release curves results in substantial misfits over as much as ~50% of the
779 cumulative ^{39}Ar. Further, we cannot predict more than 100% cumulative ^{39}Ar loss, which means
780 that the model predictions will always converge with the observations at high temperatures and
781 high cumulative ^{39}Ar release fractions.
782
783 In spite of the misfit with the cumulative ^{39}Ar release curves, we were able to estimate
784 component ages for the mixtures in case study 1 that agree with the known component ages
785 within the model credible interval, (2σ), albeit with a much larger uncertainty on the model-
786 predicted age than the known age (Table 1, Figures 6 and S3-5). In general, the ability of our
787 Bayesian model to accurately estimate the ages of individual components in the Vanlaningham
788 and Mark (2011) mixtures demonstrates that this approach can be used to extract geologically
789 meaningful age information from ^{40}Ar/^{39}Ar mixture datasets, provided that assumptions about
790 the individual components are consistent with our model framework. Moreover, these results are
791 consistent with the fact that the cumulative ^{39}Ar release curve carries less weight in our summed
792 log likelihood function than the ^{40}Ar/^{39}Ar age spectrum (Figure 5). Our ability to deconvolve
793 mixture component ages primarily from our model fits to ^{40}Ar/^{39}Ar age spectra indicates promise
794 for the broad applicability of this model framework, as many labs generating ^{40}Ar/^{39}Ar datasets
795 today heat samples with CO_2 lasers, which lack direct temperature information or control, and
796 therefore cannot quantify cumulative ^{39}Ar release as a function of temperature. That said,
797 temperature-controlled experiments are advantageous because they provide additional
798 constraints for the inversion of datasets from mixtures, whether in our Bayesian framework or in
799 a different inversion approach (e.g., Boehnke et al., 2016; Cassata et al., 2010). Furthermore,
800 although we have not done so here, accurate temperatures during step degassing can also
801 reveal information about sample-specific diffusion kinetics that can be used to inform priors.
802
803 We did not observe any systematic relationship between the uncertainty of our estimated
804 component ages and either the total number of components or the number of mineral phases
805 present. However, we did find that the relative uncertainty in our predicted ages for ACs, which
806 is significantly younger than all other components in case study 1, are ~10% or greater (2σ),
807 whereas the relative uncertainty on the ages of the other components are between 3 and 5%
808 (2σ). We hypothesize that the inflated uncertainties in the younger age component are a result

809 of the dominance of the older biotite (~ 25Ma) compared to the younger (~1 Ma) sanidine in the
810 mixture.
811
812 We also find that, although indistinguishable within the uncertainties reported, our estimated
813 ages for ACs are nominally older than the known age; likewise our estimated ages for the oldest
814 in a given mixture (either HD-B1 or TCRs) are nominally younger than the known age. We
815 hypothesize that this may result from the complexity of the dataset and the simplicity of model;
816 specifically, the assumption that each component can be described by a single domain.
817 Extending the model to account for a grain size distribution or MDD type behavior, as described
818 later in this section, may provide a more realistic model and return the known ages without bias.
819
820 *4.1.2 Case study 2*
821 Our attempts to reanalyze the Kula et al. (2010) datasets may be consistent with our
822 expectation about our Bayesian model's limits with regards to components of the same
823 mineralogy. We were unable to deconvolve the individual known component ages with the same
824 degree of prior information as we had in the Vanlaningham and Mark (2011) case study and
825 needed to impose a more restrictive prior on mixture fractions, in order to resolve two
826 components. Although we were typically able to predict the known ages of the mixture
827 components with this more restrictive prior on mixing fractions, our estimated ages are
828 characterized by very large uncertainties, particularly in comparison to the estimated age
829 uncertainties in case study 1. Furthermore, our fits to the mixture age spectra and cumulative
830 release curves had very large credible intervals in comparison to our models of the
831 Vanlaningham and Mark (2011) mixtures and miss complexity present in the observed age
832 spectra, particularly for the biotite mixtures.
833
834 In the case of the muscovite mixtures, we argue that our model's difficulty in deconvolving
835 component ages is attributable to the similarity in Ar diffusion kinetics characterizing NY25 and
836 IV14. Below ~930 ºC, the similarity in Ar diffusion kinetics is demonstrated by the significant
837 overlap between step degassing experiments of NY25 and IV14 individually both in cumulative
838 ^{39}Ar release curves (Kula et al., 2010, their figure 3) and in an Arrhenius plot (Figure S18A). At
839 temperatures > ~930 ºC, Kula et al. (2010) observe earlier gas release from IV14 muscovite
840 than NY25 muscovite in their cumulative ^{39}Ar release curves. For the muscovite mixtures, this
841 change in degassing behavior is reflected in the shape of the age spectra, first as upward
842 curvature toward the age of IV14 at intermediate to high cumulative ^{39}Ar release fractions, and

then as downward curvature at the highest ^{39}Ar gas release fractions, when Ar release from IV14 is exhausted. However, over most of the muscovite mixture age spectra, the diffusion kinetics of the two components are similar, preventing our Bayesian model from differentiating these two components.

To demonstrate the effect of similar diffusion kinetics in a true endmember case, we generated a synthetic mixture consisting of two muscovite components with the same age, grain size and mixing fraction as the 3:1 IV14:NY25 mixture. In generating the synthetic dataset for this mixture, we assume that both muscovite components are characterized by identical Ar diffusion kinetics, using the kinetic parameters from Harrison et al. (2009). The resulting synthetic age spectrum is flat and featureless with an apparent plateau age of ~130 Ma (Figure S19A), while the resulting synthetic cumulative ^{39}Ar release curve has a sigmoidal shape consistent with volume diffusion from a single phase (Figure S19B). Our mean posterior age spectrum and cumulative ^{39}Ar release curve match the synthetic data exceptionally well (Figure S19). However, like the real muscovite mixtures in case study 2, we are unable to accurately estimate both component ages in the mixture, and the older component completely dominates the mixture with an estimated mixing fraction of 92%.

Imposing more restrictive priors on the mixing fraction for the Kula et al. (2010) muscovite mixtures forced the model to discern two distinct component ages, but the predicted age for the younger component (NY25) is still in too old in the 3:1 IV14:NY25 mixture where it appears to be pinned to the final, youngest step age in the ^{40}Ar/^{39}Ar age spectrum. We hypothesize that these muscovite mixtures might be successfully deconvolved with less restrictive priors if a heating schedule with a greater number of short-duration, high-temperature steps was used. Such a heating schedule would lead to a more detailed picture of the structure of the ^{40}Ar/^{39}Ar age spectrum at high cumulative ^{39}Ar release, where the diffusion behavior of NY25 and IV14 differ the most, and therefore would increase the likelihood that our model would predict the presence of more than one component.

Our challenge deconvolving the Kula et al. (2010) biotite mixtures may also point to issues with our initial assumptions in our model framework for these mixtures. The ^{40}Ar/^{39}Ar age spectra for the Kula et al. (2010) biotite mixtures are complex, exhibiting multiple large age undulations at low ^{39}Ar release fractions and an overall decreasing age trend toward the age of the younger component at high ^{39}Ar release fractions. A decreasing age trend at high ^{39}Ar release fractions

877 is consistent with volume diffusion from two components with different ages and slightly different
878 Ar diffusion kinetics, with the younger component being more retentive than the older
879 component. This decrease toward the younger age component at the end of the experiments is
880 also consistent with the ^{39}Ar cumulative release curves observed for the individual biotite
881 components, with the younger PM1 exhibiting greater Ar loss at higher temperatures than the
882 older IV8. The large undulations in step age at lower ^{39}Ar release fractions, on the other hand,
883 are unexpected.
884
885 We propose several factors that might produce such unexpected age spectra behavior for the
886 biotite mixtures. These factors include the presence of multiple grain sizes in each component,
887 multiple diffusion domain (MDD) behavior in one or both biotite samples, non-volume diffusion
888 mechanisms, or syn-experiment structural breakdown of biotite. Effects associated with the
889 presence of multiple grain sizes are possible, although we view this as unlikely to explain these
890 undulations entirely as the range of sieve sizes used by Kula et al. (2010) was small (177-250
891 μm). Similarly, syn-experiment structural breakdown due to heating is unlikely to produce such
892 undulations, as both biotite or muscovite samples would be expected to undergo crystal-
893 chemical changes at similar temperatures and therefore steps in these experiments. A
894 component of non-volume diffusion and/or MDD-like behavior remain possibilities and are
895 consistent with the observed cumulative ^{39}Ar release curves and Arrhenius relationships for the
896 individual biotite components, IV8 and PM1. Instead of exhibiting the characteristic sigmoidal
897 shape diagnostic of volume diffusion (e.g., McDannell et al., 2018), the cumulative ^{39}Ar release
898 curves for IV8 and PM1 individually are relatively straight until high release fractions, whereby
899 definition values have to approach 100%. The Arrhenius plots of diffusivities for these individual
900 biotite components (Figure S18C) exhibit a curvilinear pattern, indicative of the presence of
901 multiple domains (e.g., Lovera et al., 1989), rather than linear arrays as expected for thermally-
902 driven volume diffusion from a single domain, and as observed for most of the cumulative gas
903 released from the muscovite samples.
904
905 For any of these potential explanations for the biotite mixture age spectra behaviour, the initial
906 assumptions of the current Bayesian model framework are violated. Specifically, we have
907 assumed a single grain size and simple, single-domain volume diffusion with no structural
908 transformations or changes in Ar diffusion kinetics for each component. Therefore, as we can
909 see from the posterior age spectra (Figures 7-8, A-C) our models inability to capture the
910 undulations, but it does predict the decrease toward the younger age components at high

911 cumulative ^{39}Ar release fractions for all three biotite mixtures. These effects may also be
912 affecting our model's ability to reproduce the muscovite mixture datasets, although this is likely
913 to a smaller extent as the undulations observed in the muscovite age spectra are much more
914 subtle.
915
916 In applications of our Bayesian model to geologic samples, it may be difficult to identify when
917 the model's underlying assumptions about the individual components, such as only volume
918 diffusion from a single domain, are violated, particularly if used to analyze mixtures with many
919 more than two components. However, we also demonstrated that using additional constraints
920 such as mixing fractions enabled us to nonetheless obtain reasonable estimates of the
921 component ages in the biotite and muscovite mixtures in most cases, even if we were unable to
922 entirely capture the complexity in the mixtures' age spectra. This additional constraint on
923 mixture fraction may not be unreasonable for some geologic applications. For example, IV8 has
924 higher Fe but much lower Mg contents than PM1 (Kula et al. 2010). We therefore could have
925 determined that there were two different biotite populations in the Kula et al. (2010) mixtures
926 and in roughly what proportions they occur from compositional information independent of the
927 Ar measurements. Therefore, although some real mixtures may have components that violate
928 our model's underlying assumptions, we may still be able to extract meaningful
929 geochronological information using our Bayesian approach, particularly if we have more prior
930 information to incorporate into the model framework.
931
932 *4.1.3 Case study 3*
933 Case studies 1 and 2 highlight some of the strengths and weaknesses of our Bayesian
934 approach to deconvolving $^{40}Ar/^{39}Ar$ datasets but lack geological significance in that the mixtures
935 we deconvolved were laboratory-generated. Case study 3 is intended to provide a geologically
936 interesting example: the analyses of bulk material from a planetary surface regolith. Although
937 also artificial, we generated a hypothetical $^{40}Ar/^{39}Ar$ dataset for a Martian surface sample to
938 highlight the complexity of estimating geologically relevant age information from potential *in situ*
939 planetary measurements, or measurements on bulk material from meteorites or returned
940 samples. Although real datasets for lunar and Martian samples with multiple components exist,
941 at present our model does not strictly accommodate MDD-type behavior for individual
942 components, which is frequently exhibited in these data sets; therefore testing our models on
943 these datasets would probably not be informative without improvements to the model framework
944 (see section 4.3.2).

The synthetic age spectrum in this case study shows monotonically increasing step ages to an apparent plateau encompassing the last ~70% of the cumulative ^{39}Ar released. As discussed previously, this age spectrum pattern would conventionally be interpreted as reflecting partial diffusive loss of $^{40}Ar^*$, but for this mixture actually represents the simultaneous degassing of Ar from minerals (jarosite, plagioclase, and sanidine) with different ages and Ar diffusion kinetics. Like in case study 1, the very good fit we observe with the age spectrum for the synthetic Martian mixture reflects the fact that this mixture satisfies the assumptions underlying the Bayesian model setup. Unlike case study 1, for which we suspect issues with the furnace calibration at low temperature, we also observe good agreement between the synthetic Martian ^{39}Ar cumulative release curve, and the Bayesian mean posterior model (Fig. 9C). These results are not unexpected for case study 3, as we have defined the diffusion kinetics grain size for each component in the mixture, and we do not introduce non-ideal behaviour such as complex diffusion behaviour (e.g., MDD) or non-volume diffusion. The idealized parameters we chose also enable us to deconvolve the component ages in this synthetic mixture within the uncertainty of the known component ages. However, as our synthetic muscovite mixture from case study 2 demonstrates (Figure S19 and Table S1), our ability to deconvolve the component ages is not a self-fulfilling outcome of generating a synthetic dataset and is dependent on the individual components of the synthetic mixture, having non-identical Ar diffusion kinetics.

One potential limitation of this case study is that we have not included a non-negligible amorphous K-bearing component (e.g., feldspathic glass), which has been observed in Murray Formation mudstones (Rampe et al., 2017) and which may carry geologically relevant age information. It is possible to include an amorphous phase within this model as diffusion studies of glass have been carried out previously (e.g., Cassata et al., 2010; Gombosi et al., 2015). However, the diffusion kinetics of amorphous materials have not been extensively studied and as such uninformative priors would need to be constructed for these parameters to reflect this limited knowledge.

4.2 Comparison to other approaches

Cassata et al. (2010) and Boehnke et al. (2016) have recently presented models for fitting and inferring information from age spectra from the degassing of multi-component mixtures. Our Bayesian approach is similar to theirs in that we assume each mixture is comprised of multiple components characterized by different Ar diffusion kinetics, which is analogous way that MDD

979 modeling assumes that crystals are comprised of multiple domains with distinct diffusion kinetics
980 of individual components. However, both Cassata et al. (2010) and Boehnke et al. (2016)
981 incorporate MDD-type behaviour for individual components, which is an often-observed property
982 of framework silicates (McDougall and Harrison, 1999). Our Bayesian framework can accurately
983 represent MDD-type behavior: each domain in a particular mineral exhibiting MDD behavior will
984 be represented as a component with a distinct age and Ar diffusion kinetics in the model
985 posterior. However, because the framework as we implemented it here uses the number of
986 components as a prior, we are assuming that MDD-type behavior is not occurring and that each
987 component can be accurately represented with a single diffusion domain. Our assumption of
988 simple diffusion behavior for individual components may contribute to our challenges in
989 deconvolving age components for mica mixtures in case study 2. We describe in greater detail
990 below how this assumption can be removed using a non-parametric framework in future work.
991
992 There are several major advantages of our Bayesian approach over those of Cassata et al.
993 (2010) and Boehnke et al. (2016). First, in contrast to Cassata et al. (2010) our approach allows
994 parameters like diffusion kinetics to be constrained by the model inversion rather than
995 subjectively imposed. Furthermore, the Bayesian approach enables us to directly quantify the
996 uncertainty of all model parameters by their description as posterior probability distribution
997 functions. This is distinct from the approach of Boehnke et al. (2016), the most flexible existing
998 framework for multi-component $^{40}Ar/^{39}Ar$ analysis, which cannot quantify uncertainties of model
999 parameters due to the computational complexity of the approach (Boehnke et al., 2016).
1000 However, unlike Boehnke et al. (2016) we do not jointly optimize the Arrhenius plot and age
1001 spectrum, nor have we incorporated MDD-type behaviour for individual components. As many
1002 samples exhibit Ar diffusion with MDD-type behavior, incorporating this type of behavior is one
1003 of the ways we can improve our model framework, which we discuss in more detail below.
1004
1005 **4.3 Future Work**
1006 *4.3.1 Observational improvements*
1007 As previously mentioned, one potential reason why we were more successful in deconvolving
1008 the mixtures in case study 1 than in case study 2 may be the number of steps in the heating
1009 experiment and the resulting structure of the $^{40}Ar/^{39}Ar$ age spectra. The age spectra in case
1010 study 1 are characterized by many more temperature steps than the age spectra in case study
1011 2, which allows finer scale structure in the age spectra to be observed in case study 1. As noted
1012 by Gillespie et al., (1982) and Dong et al., (2000), differing diffusion kinetics between mixture

components can allow Ar release from each component in the mixture to be unmixed via thermal separation, as the less retentive phases will experience greater degassing at lower temperatures than more retentive phases (e.g., Fig. 10). Degassing mineral mixtures over a greater number of steps and over smaller increments of temperature change should therefore enhance this thermal separation. We therefore suggest that, ideally, a very detailed heating schedule (>50 steps) coupled with our Bayesian approach has the greatest potential for success when deconvolving multi-component mixtures. In addition to degassing mixtures over many steps, other heating schedule strategies such as isothermal and retrograde heating steps, as noted by Harrison et al. (1991), should further help in unmixing the Ar contributed from each component in a mixture.

In addition to optimizing step heating experiments, we can pair mixture age spectrum data with other observations to place more informed constraints on priors in our model framework. Priors are one of the most important ingredients in the Bayesian framework, as they express our state of knowledge about a parameter before data is observed and constrain the posterior space of the model to a space smaller than that allowed by the likelihood itself. The age priors used in the case studies presented here are as uninformative as possible: a uniform distribution between 0 and 4.6 Ga. A uniform prior such as this does not affect the landscape of the posterior. By providing more informed priors in our model setup, it is possible to both increase model efficiency and yield better constraints on the posterior distributions of model parameters. For example, XRD information on mineral mixtures can be used to constrain the mineral phases that make up the mixture. This information about minerals present can be used to both optimize heating schedules for step heating experiments and use more informed priors for the diffusion kinetics characterizing each component in the inversion setup. Additionally, for real geological samples we can incorporate geologic context into our prior for mineral component ages. For example, if we have a sample from a terrestrial setting in a particular stratigraphic unit of known age, we can constrain the ages of components to be equal to or greater than the stratigraphic age. Similarly, in many cases we will have constraints on the range of potential source ages of sediment in a basin setting that can be used to better define age priors. Age priors such as this are frequently utilized in Bayesian radiocarbon modelling (Ramsey, 2009) and can be readily incorporated into the Bayesian framework presented here.

4.3.2 Model improvements

Our three case studies highlight the advantages and shortcomings of our Bayesian approach and areas where implementing modifications to the model framework can improve fits to $^{40}Ar/^{39}Ar$ datasets as well as confidence in the estimated parameters of interest like component age. As discussed above, we think that one of the biggest challenges we faced modeling the age spectra, cumulative release curves, and component ages in case study 2 may be MDD-like behavior. In the current model framework, we cannot account for MDD-like behavior if it occurs within a component as we have defined it. In non-artificial mixtures, we will also likely need to account for grain size variation and its effect on diffusion kinetics, which will have a similar effect to MDD-like behavior. However, as discussed above, we may not have information about the presence of MDD-like behavior *a priori*, nor may we have detailed constraints on the grain size distribution in some mixtures (e.g., *in situ* planetary measurements or bulk meteorite analyses).

Having *a priori* knowledge of either MDD-like behaviour or the grain size distribution of a mixture component may not be necessary if we modify our Bayesian framework to be nonparametric. In such a modelling framework, the number of variables represents an unknown to be inferred (i.e., the underlying grain size distribution or the number of domains). Given that our datasets are both non-negative and compositional, we can utilize mixture models in which our observations are some linear combination of end member processes. Mixture models have been widely utilized in detrital geochronology (Sambridge and Compston, 1994) and grain size distribution studies (Yu et al., 2016), which are also non-negative and compositional in nature. The Dirichlet process is one way to implement nonparametric statistics and is used primarily in Gaussian mixture models where the number of Gaussian distributions is unknown (Ferguson, 1973; Sethuraman, 1994). Another nonparametric approach is to use a reversible jump Markov Chain Monte Carlo (RJMCMC) algorithm, where the number of model parameters is allowed to vary between model time steps (e.g., Gallagher et al., 2012). Both Dirichlet and RJMCMC methods can be readily implemented into our existing Bayesian framework, although both methods will make our Bayesian model substantially more computationally expensive (approximately an order of magnitude slower, based on preliminary implementations).

Regardless of implementation of a nonparametric Bayesian framework, we can also place additional constraints on the age prior for components using the method of asymptotes formulated by Forster and Lister (2003). In their interpretation, an upward-converging age

asymptote, or partial pseudo plateau, represents the minimum age of one component, while a downward-converging asymptote represents a maximum age of another. Although the presence of asymptotes provides only lower or upper bounds on the age of components, we could potentially use this method of bounds to restrict the prior space for the age components. For example, Mixture 1 in case study 1 (Fig. 1) exhibits a downward asymptoting plateau at ~2 Ma which could be interpreted as a maximum age for the more retentive ACs component, thus allowing the age priors to be restricted between 0-2 Ma rather than 0 - 4.6 Ga. Similarly, the initial pseudo plateau at ~12 Ma could be interpreted as a minimum age for the HD-B1 component, restricting the prior age for this component between 12 Ma - 4.6 Ga. Placing a narrower uniform distribution on the prior age for the ACs component may enable us to reduce the uncertainty in our posterior age estimate, which was elevated for this component relative to the other, older components in case study 1. In general, using asymptotes as a constraint may increase our model efficiency and potentially improve our estimates of posterior distributions of model parameters.

A final improvement we envision for our Bayesian model framework is to fit additional parameters, such as the K/Ca ratios calculated from step heating experiments. K-bearing minerals have ranges of K/Ca ratios that can be included as prior information (e.g., McDougall and Harrison, 1999). Since K/Ca spectra will depend on many of the same model parameters as age spectra and cumulative release curves (e.g., a, E_a, D_0, ϕ), by including this observation we anticipate being able to better constrain the posterior distributions of these model parameters, as well as model parameters such as component ages.

In summary, although our Bayesian framework as implemented here can be used to successfully deconvolve $^{40}Ar/^{39}Ar$ datasets from mineral mixtures, we can add additional model constraints to further improve our posterior estimates of model parameters, as well as make our model framework more flexible to accommodate $^{40}Ar/^{39}Ar$ datasets from more complex mixtures.

4.4 Applications

There are several geological applications for which obtaining $^{40}Ar/^{39}Ar$ datasets from polymineralic samples are useful or necessary. In these circumstances, the conventional 'plateau' criteria often used to interpret $^{40}Ar/^{39}Ar$ datasets is of limited or no value. Our Bayesian approach provides a quantitative interpretive framework that can yield geologically meaningful age information from multi-component samples. We envision the Bayesian approach being

particularly useful for are (1) provenance studies of fine-grained sediments and (2) dating of terrestrial and extraterrestrial materials, both *in situ* by exploration vehicles or analysis of returned samples and meteorites.

In provenance studies, conventional sample preparation approaches may be undesirable for fine-grained sediment samples, especially in the case of silt sized material (~20-63 μm) whereby the processes of acid leaching or picking under an optical microscope, could result in grain size biasing or loss of sample. In such a setting conventional K-Ar ages or $^{40}Ar/^{39}Ar$ fusion ages will reflect the integrated $^{40}Ar/^{39}Ar$ ages of all the sediment sources, and therefore not provide geologically meaningful information. Through the use of detailed stepwise heating coupled with our Bayesian approach, the ages corresponding to different sources could be estimated, and in cases where the potential source bedrock ages are known the presence or absence and possibly even the proportion of a particular provenance signal can be determined. Using our Bayesian approach could therefore be fruitful in provenance studies of loess (e.g., China Loess Plateau), submarine fan systems (e.g., Bengal Fan) and sediments that result from megaflood events (e.g., channeled scablands of North America) where fine-grained sediments will dominate. One important caveat is that application of $^{40}Ar/^{39}Ar$ dating to fine-grained material could be susceptible to recoil. It has been shown that ^{39}Ar can recoil ca. 0.08 μm (Onstott et al. 1995) and therefore can be problematic for $^{40}Ar/^{39}Ar$ dating of fine-grained materials. There is no doubt that reactor-induced ^{39}Ar and ^{37}Ar recoil will limit the application of our approach. However, as identified by Vanlaningham and Mark (2011) we do not expect recoil to be a major issue if samples are sonicated (to remove clay-sized particles adhered to coarser grains) and sieved at 10 μm and larger. Furthermore, we could build on knowledge from previous studies (e.g., Onstott et al. 1995; Paine et al. 2006; Jourdan et al. 2007) and incorporate the effects of recoil on the initial distribution of ^{39}Ar and ^{37}Ar explicitly into our model framework, which would allow us to apply this framework to the finest-grained provenance archives without resorting to micro-encapsulation techniques that allow for direct measurement of recoiled ^{39}Ar and ^{37}Ar (Dong et al. 1995). Nevertheless, if possible, experiments designed to utilise our Bayesian model should interrogate a range of grain-sizes common to all samples of interest, including the coarsest fractions which are not susceptible to recoil.

In addition to the use as a provenance tool, our Bayesian approach could also be particularly useful for geochronology of planetary materials, both in the unlikely case of *in situ* planetary geochronology and, more prevalently, in the analysis of meteorites or mission-returned samples

that are too fine-grained or valuable to carry out mineral separation. In the only *in situ* approach, the dating of the Martian regolith, the Curiosity rover SAM suite was used for analysis and the sample preparation was limited to simple sieving before SAM analysis. Detailed XRD analysis prior to the analysis revealed that in both cases multiple K-bearing components were constituents of the regolith (e.g., jarosite, and plagioclase). Given this limited sample preparation, by default, the samples must be of a polymineralic nature; however, what is not known is the geological age(s) of the K-bearing components. An attempt was made by Martin et al. (2017) to thermally separate K-components by employing a two-step heating method. In this analysis the low temperature step preferentially degassed the less retentive, younger component, inferred to be jarosite, and the high temperature step degassed a more retentive and older component, inferred to be detrital feldspar. However, despite the success of these applications the K-Ar ages inferred are only as accurate as the underlying assumptions that are coupled with them. Our Bayesian approach has the potential to interrogate extraterrestrial surfaces more thoroughly extracting ages of the K-bearing components in the Martian surface. As mentioned above the application of XRD priors to analysis would allow for the creation of prior probability density functions for mineral specific information (i.e., E_a, D_0, ϕ, *K/Ca),* furthermore the process of sieving will create bounds on the grain size priors. We highlight such an example in case study 3 which provides an idealised synthetic $^{40}Ar/^{39}Ar$ dataset of the Martian regolith of three different K-bearing components and ages; jarosite (2.1 Ga), plagioclase (4.3 Ga), and sanidine (4.1 Ga). This idealised case study highlights the applicability of our Bayesian analytical method to extract geologically meaningful ages from *in situ* rocky body settings.

5. CONCLUSIONS

Currently the $^{40}Ar/^{39}Ar$ dating system is most commonly applied to either single mineral phases or groundmass analysis. However, there are geological settings and problems where the analysis of mixtures with multiple components will be desirable or necessary, and such mixture data requires a nonconventional approach to estimate the age(s) of each of the components that constitute the mixture. We have developed a Bayesian approach to address this problem, which first consists of constructing a multiple component age equation then inverting an $^{40}Ar/^{39}Ar$ dataset within this multi-component age framework to estimate the desired model parameters, i.e., the age of each component.

With our Bayesian approach, we find that there is more information available in mixed age spectra than previously realised, although our approach also has limitations. Our reanalysis of the mixtures of monitor standards created by Vanlaningham and Mark (2011) demonstrates that our model does a reasonably good job of fitting observed $^{40}Ar/^{39}Ar$ age spectra from mixtures, but generally does not reproduce cumulative ^{39}Ar release curves. We argue that the misfit with the latter is likely a consequence of inaccuracies in the calibration of the furnace used by Vanlaningham and Mark (2011) at low temperatures. Of most significance, our reanalysis demonstrates that, with prior knowledge of the number of components and the mineral phases present, the ages of individual components can be inverted from $^{40}Ar/^{39}Ar$ datasets resulting from bulk mixtures. The ability of our model to invert individual component ages is a consequence of these mixtures meeting the assumptions we set forth in the model setup.

Our reanalysis of the biotite and muscovite mixtures created by Kula et al., (2010) presents a limiting case for our modeling approach. Specifically, we were unable to resolve multiple components in the Kula et al. (2010) mixtures with the same degree of prior information used to invert the Vanlaningham and Mark (2011) mixtures. In addition to prior knowledge of the number of components and mineral phases present, we also had to place narrower prior constraints on the mixing fractions in order to accurately resolve more than one component. With this additional prior information, we improved our estimates of the age components and resolved the known ages in all but one case, the younger component (NY25) in the 3:1 IV14:NY25 mixture. In all estimated ages we see an inflated uncertainty compared with both case study 1 and case study 3. We hypothesise that this is largely due to the similarity in Ar diffusion kinetics between the components in the Kula et al. (2010) muscovite mixtures. There may also be issues associated with the assumptions in our model setup, including potential MDD-like or non-volume diffusion behavior, particularly for the biotite mixtures. It is also possible that, for these mixtures, a more detailed heating schedule that better resolves the structure of the $^{40}Ar/^{39}Ar$ age spectrum would improve the performance of our Bayesian model.

In addition to reanalyzing mixtures created in the laboratory, we also present an example hypothetical application of our Bayesian approach for deconvolving an $^{40}Ar/^{39}Ar$ age spectrum from *in situ* measurements on Mars. This synthetic dataset, which we generated from existing Martian geochronological and mineralogical data, strongly resembles an $^{40}Ar/^{39}Ar$ age spectrum for a single component sample that has experienced diffusive loss. Nonetheless, we are able to use our Bayesian model to predict the $^{40}Ar/^{39}Ar$ age spectrum and cumulative ^{39}Ar release

curve, as well as determine the component ages, of the synthetic dataset. Our example therefore highlights how our Bayesian approach could be used to distinguish between different possible interpretations of complex age spectra when multiple components are present. We propose that the Bayesian framework presented herein could allow the utilisation of $^{40}Ar/^{39}Ar$ as a provenance tool for fine-grained sediments, as well as for geochronology studies of meteorites and mission-returned samples from rocky bodies in the inner Solar System.

ACKNOWLEDGEMENTS

JNC was supported by a case studentship from the UK Space Agency (UKSA). NERC are thanked for ongoing support of the National Environmental Isotope Facility $^{40}Ar/^{39}Ar$ laboratory at SUERC. We thank Clare Warren for suggesting we use the Kula et al. (2010) dataset as a case study for our Bayesian method. In addition, we would like to thank Ross Dymock for technical support.

REFERENCES CITED

Anderson, R. C., Jandura, L., Okon, A., Sunshine, D., Roumeliotis, C., Beegle, L., Hurowitz, J., Kennedy, B., Limonadi, D., McCloskey, S., et al. (2012). Collecting samples in gale crater, Mars; an overview of the Mars science laboratory sample acquisition, sample processing and handling system. *Space Science Reviews*, 170(1-4): 57–75.

Baxter, E. F. (2010). Diffusion of noble gases in minerals. *Reviews in Mineralogy and Geochemistry,* 72(1):509–557.

Boehnke, P., Harrison, T. M., Heizler, M., and Warren, P. (2016). A model for meteoritic and lunar $^{40}Ar/^{39}Ar$ age spectra: Addressing the conundrum of multi-activation energies. *Earth and Planetary Science Letters*, 453: 267–275.

Cassata, W. S. (2014). In situ dating on mars: A new approach to the K–Ar method utilizing cosmogenic argon. *Acta Astronautica*, 94(1): 222–233.

Cassata, W. S. and Renne, P. R. (2013). Systematic variations of Argon diffusion in feldspars and implications for thermochronometry. *Geochimica et Cosmochimica Acta*, 112: 251–287.

Cassata, W. S., Renne, P. R., and Shuster, D. L. (2009). Argon diffusion in plagioclase and implications for thermochronometry: a case study from the Bushveld complex, South Africa. *Geochimica et Cosmochimica Acta*, 73(21): 6600–6612.

Cassata, W. S., Shuster, D. L., Renne, P. R., and Weiss, B. P. (2010). Evidence for shock heating and constraints on martian surface temperatures revealed by $^{40}Ar/^{39}Ar$ thermochronometry of Martian meteorites. *Geochimica et Cosmochimica Acta*, 74(23):6900–6920.

Cassata, W.S., Cohen, B.E., Mark, D.F., Trappitsch, R., Crow, C.A., Wimpenny, J., Lee, M.R. and Smith, C.L., 2018. Chronology of Martian breccia NWA 7034 and the formation of the Martian crustal dichotomy. *Science advances*, *4*(5), p.eaap8306.

Cho, Y., Horiuchi, M., Shibasaki, K., Kameda, S., and Sugita, S. (2017). Quantitative potassium measurements with laser-induced breakdown spectroscopy using low-energy lasers: Application to in situ K–Ar geochronology for planetary exploration. *Applied spectroscopy*, 71(8):1969–1981.

Cohen, B. A., Swindle, T., and Roark, S. (2014). In situ geochronology on the Mars 2020 rover with KARLE (potassium-argon laser experiment).

Copeland, P. and Harrison, T. M. (1990). Episodic rapid uplift in the Himalaya revealed by $^{40}Ar/^{39}Ar$ analysis of detrital K-feldspar and muscovite, Bengal fan. *Geology*, 18(4):354–357.

Crank, J., 1975. The mathematics of diffusion 2nd Edition. *Oxford Science Publications*, p.32.

Diebolt, J. and Robert, C. P. (1994). Estimation of finite mixture distributions through Bayesian sampling. *Journal of the Royal Statistical Society. Series B (Methodological*), *56(2)*, pp. 363–375.

Dong, H., Hall, C.M., Peacor, D.R., Halliday, A.N. and Pevear, D.R., 2000. Thermal $^{40}Ar/^{39}Ar$ separation of diagenetic from detrital illitic clays in Gulf Coast shales. *Earth and Planetary Science Letters*, *175*(3-4), pp.309-325.

Duane, S., Kennedy, A. D., Pendleton, B. J., and Roweth, D. (1987). Hybrid monte carlo. *Physics letters B*, 195(2), pp.216–222.

Ehlmann, B. L. and Edwards, C. S. (2014). Mineralogy of the Martian surface. *Annual Review of Earth and Planetary Sciences*, 42, pp.291–315.

Farley, K., Malespin, C., Mahaffy, P., Grotzinger, J., Vasconcelos, P., Milliken, R., Malin, M., Edgett, K., Pavlov, A., Hurowitz, J., et al. (2014). In situ radiometric and exposure age dating of the Martian surface. *science*, 343(6169), p.1247166.

Fechtig, H. and Kalbitzer, S. (1966). The diffusion of Argon in Potassium-bearing solids. *In Potassium argon dating* (pp.68–107). Springer, Berin, Heidelberg.

Ferguson, T.S., 1973. A Bayesian analysis of some nonparametric problems. *The annals of statistics*, pp.209-230.

Fleck, R. J., Sutter, J. F., and Elliot, D. H. (1977). Interpretation of discordant $^{40}Ar/^{39}Ar$ age-spectra of Mesozoic tholeiites from Antarctica. *Geochimica et Cosmochimica Acta*, *41*(1), pp.15–32.

Foland, K. (1994). Argon diffusion in feldspars. In *Feldspars and their reactions*,(pp. 415–447). Springer, Dordrecht.

Forster, M. and Lister, G. (2004). The interpretation of $^{40}Ar/^{39}Ar$ apparent age spectra produced by mixing: application of the method of asymptotes and limits. *Journal of Structural Geology*, *26*(2), pp.287–305.

Gaber, L.J., Foland, K.A. and Corbato, C.E., 1988. On the significance of argon release from biotite and amphibole during $^{40}Ar/^{39}Ar$ vacuum heating. *Geochimica et Cosmochimica Acta*, *52*(10), pp.2457-2465.

Gallagher, K., Charvin, K., Nielsen, S., Sambridge, M., and Stephenson, J. (2009). Markov Chain Monte Carlo (MCMC) sampling methods to determine optimal models, model resolution and model choice for earth science problems. *Marine and Petroleum Geology*, *26*(4), pp.525–535.

Gallagher, K., 2012. Transdimensional inverse thermal history modeling for quantitative thermochronology. *Journal of Geophysical Research: Solid Earth*, *117*(B2).

Gelman, A., Stern, H. S., Carlin, J. B., Dunson, D. B., Vehtari, A., and Rubin, D. B. (2013*). Bayesian data analysis*. CRC press.

Gillespie, A., Huneke, J., and Wasserburg, G. (1982). An assessment of $^{40}Ar/^{39}Ar$ dating of incompletely degassed xenoliths. *Journal of Geophysical Research: Solid Earth, 87*(B11), pp.9247–9257.

Gombiner, J.H., Hemming, S.R., Hendy, I.L., Bryce, J.G. and Blichert-Toft, J., 2016. Isotopic and elemental evidence for Scabland Flood sediments offshore Vancouver Island. *Quaternary Science Reviews*, *139*, pp.129-137.

Gombosi, D.J., Baldwin, S.L., Watson, E.B., Swindle, T.D., Delano, J.W., Roberge, W.G., 2015. Argon diffusion in Apollo 16 impact glass spherules: Implications for $^{40}Ar/^{39}Ar$ dating of lunar impact events. *Geochimica et Cosmochimica Acta* 148, 251–268.

Harrison, T.M., Célérier, J., Aikman, A.B., Hermann, J., Heizler, M.T., 2009. Diffusion of ^{40}Ar in muscovite. *Geochimica et Cosmochimica Acta* 73, 1039–1051.

Harrison, T. M., Duncan, I., and McDougall, I. (1985). Diffusion of ^{40}Ar in biotite: temperature, pressure and compositional effects. *Geochimica et Cosmochimica Acta, 49*(11), pp.2461–2468.

Harrison, T. M., Lovera, O. M., and Matthew, T. H. (1991). $^{40}Ar/^{39}Ar$ results for alkali feldspars containing diffusion domains with differing activation energy. *Geochimica et Cosmochimica Acta, 55*(5), pp.1435–1448.

Hemming, S., Broecker, W., Sharp, W., Bond, G., Gwiazda, R., McManus, J., Klas, M., and Hajdas, I. (1998). Provenance of Heinrich layers in core V28-82, northeastern Atlantic: $^{40}Ar/^{39}Ar$ ages of ice-rafted hornblende, Pb isotopes in feldspar grains, and Nd–Sr–Pb isotopes in the fine sediment fraction. *Earth and Planetary Science Letters, 164*(1-2), pp.317–333.

Hoffman, M. D. and Gelman, A. (2014). The No-U-Turn sampler: adaptively setting path lengths in Hamiltonian Monte Carlo. *Journal of Machine Learning Research, 15*(1), pp.1593–1623.

Idleman, B. D., Zeitler, P. K., and McDannell, K. T. (2018). Characterization of helium release from Apatite by continuous ramped heating. *Chemical Geology*, *476*, pp.223–232.

Jourdan, F., Matzel, J.P. and Renne, P.R., 2007. ^{39}Ar and ^{37}Ar recoil loss during neutron irradiation of sanidine and plagioclase. *Geochimica et Cosmochimica Acta*, 71(11), pp. 2791-2808.

Kelley, S. (2002). Excess argon in K–Ar and Ar–Ar geochronology. *Chemical Geology, 188*(1-2), pp.1–22.

Kula, J. and Baldwin, S. L. (2011). Jarosite, Argon diffusion, and dating aqueous mineralization on Earth and Mars. *Earth and Planetary Science Letters, 310*(3- 4), pp.314–318.

Kula, J., Spell, T. L., and Zanetti, K. A. (2010). $^{40}Ar/^{39}Ar$ analyses of artificially mixed micas and the treatment of complex age spectra from samples with multiple mica populations. *Chemical Geology, 275*(1-2), pp.67–77.

Lanphere, M. A. and Dalrymple, G. B. (1976). Identification of excess ^{40}Ar by the $^{40}Ar/^{39}Ar$ age spectrum technique. *Earth and Planetary Science Letters, 32*(2), pp.141–148.

Lovera, O. M., Grove, M., and Harrison, T. M. (2002). Systematic analysis of K-feldspar $^{40}Ar/^{39}Ar$ step heating results II: Relevance of laboratory argon diffusion properties to nature. *Geochimica et Cosmochimica Acta, 66*(7), pp.1237– 1255.

Lovera, O. M., Richter, F. M., and Harrison, T. M. (1989). The $^{40}Ar/^{39}Ar$ thermochronometry for slowly cooled samples having a distribution of diffusion domain sizes. *Journal of Geophysical Research: Solid Earth, 94*(B12), pp.17917– 17935.

Lovera, O. M., Richter, F. M., and Harrison, T. M. (1991). Diffusion domains determined by ^{39}Ar released during step heating. *Journal of Geophysical Research: Solid Earth, 96*(B2), pp.2057–2069.

Mahaffy, P. R., Webster, C. R., Cabane, M., Conrad, P. G., Coll, P., Atreya, S. K., Arvey, R., Barciniak, M., Benna, M., Bleacher, L., et al. (2012). The sample analysis at Mars investigation and instrument suite. *Space Science Reviews, 170*(1-4), pp.401–478.

Mark, D., Barfod, D., Stuart, F., and Imlach, J. (2009). The ARGUS multicollector noble gas mass spectrometer: Performance for $^{40}Ar/^{39}Ar$ geochronology. *Geochemistry, Geophysics, Geosystems, 10*(10).

Mark, D.F., Renne, P.R., Dymock, R.C., Smith, V.C., Simon, J.I., Morgan, L.E., Staff, R.A., Ellis, B.S. and Pearce, N.J., 2017. High-precision 40Ar/39Ar dating of Pleistocene tuffs and temporal anchoring of the Matuyama-Brunhes boundary. *Quaternary Geochronology*, *39*, pp.1-23.

Martin, P., Farley, K., Baker, M., Malespin, C., Schwenzer, S., Cohen, B., Mahaffy, P., McAdam, A., Ming, D., Vasconcelos, P., et al. (2017). A two-step K-Ar experiment on mars: Dating the diagenetic formation of jarosite from Amazonian groundwaters. *Journal of Geophysical Research: Planets, 122*(12), pp.2803–2818.

McDougall, I., Mac Dougall, I., Harrison, T. M., et al. (1999). *Geochronology and Thermochronology by the $^{40}Ar/^{39}Ar$ Method*. Oxford University Press on Demand.

McDougall, I. and Wellman, P. (2011). Calibration of GA1550 biotite standard for K/Ar and $^{40}Ar/^{39}Ar$ dating. *Chemical Geology, 280*(1-2), pp.19–25.

Merrihue, C. and Turner, G. (1966). Potassium-argon dating by activation with fast neutrons. *Journal of Geophysical Research, 71*(11), pp.2852–2857.

Metropolis, N., Rosenbluth, A. W., Rosenbluth, M. N., Teller, A. H., Teller, E., et al. (1953). Equation of state calculations by fast computing machines. *J. Chem. Phys, 21*(6), pp.1087–1092.

Morgan, L.E., Mark, D.F., Imlach, J., Barfod, D. and Dymock, R., 2014. FCs-EK: A new sampling of the Fish Canyon Tuff 40Ar/39Ar neutron flux monitor. *Geological Society, London, Special Publications*, *378*(1), pp.63-67.

Morgan, L. E., Munk, M., Davidheiser-Kroll, B., Warner, N. H., Gupta, S., Slaybaugh, R., Harkness, P., and Mark, D. F. (2017). Instrumentation development for in situ $^{40}Ar/^{39}Ar$ Planetary Geochronology. *Geostandards and Geoanalytical Research, 41*(3), pp.381–396.

Onstott, T., Miller, M., Ewing, R., Arnold, G., and Walsh, D. (1995). Recoil refinements: Implications for the $^{40}Ar/^{39}Ar$ dating technique. *Geochimica et Cosmochimica Acta, 59*(9), pp.1821–1834.

Paine, J.H., Nomade, S. and Renne, P.R., 2006. Quantification of 39Ar recoil ejection from GA1550 biotite during neutron irradiation as a function of grain dimensions. *Geochimica et Cosmochimica Acta*, *70*(6), pp.1507-1517.

Patterson, C. (1956). Age of meteorites and the earth. *Geochimica et Cosmochimica Acta, 10*(4), pp.230–237.

Preece, K., Mark, D. F., Barclay, J., Cohen, B. E., Chamberlain, K. J., Jowitt, C., Vye-Brown, C., Brown, R. J., and Hamilton, S. (2018). Bridging the gap: $^{40}Ar/^{39}Ar$ dating of volcanic eruptions from the 'Age of Discovery'. *Geology, 46*(12), pp.1035–1038.

Rampe, E.B., Ming, D.W., Morris, R.V., Blake, D.F., Bristow, T.F., SJ, C., Vaniman, D.T., Yen, A.S., Grotzinger, J.P., Downs, R.T. and Des Marais, D.J., 2016. Diagenesis in the Murray formation, Gale Crater, Mars.

Ramsey, C. B. (2009). Bayesian analysis of radiocarbon dates. *Radiocarbon, 51*(1), pp.337–360.

Renne, P., Sharp, W., Deino, A., Orsi, G., and Civetta, L. (1997). $^{40}Ar/^{39}Ar$ dating into the historical realm: Calibration against Pliny the Younger. *Science, 277*(5330), pp.1279–1280.

Renne, P.R., Swisher, C.C., Deino, A.L., Karner, D.B., Owens, T.L. and DePaolo, D.J., 1998. Intercalibration of standards, absolute ages and uncertainties in 40Ar/39Ar dating. *Chemical Geology*, *145*(1-2), pp.117-152.

Renne, P. R. (2000). $^{40}Ar/^{39}Ar$ age of plagioclase from Acapulco meteorite and the problem of systematic errors in cosmochronology. *Earth and Planetary Science Letters*, 175(1-2), pp.13–26.

Rex, D., Guise, P., and Wartho, J.-A. (1993). Disturbed $^{40}Ar/^{39}Ar$ spectra from hornblendes: Thermal loss or contamination. *Chemical Geology, 103*(1- 4), pp.271–281.

Salvatier, J., Wiecki, T. V., and Fonnesbeck, C. (2016). Probabilistic programming in Python using PyMC3*. PeerJ Computer Science, 2*, p.e55.

Sambridge, M. and Compston, W. (1994). Mixture modeling of multi- component data sets with application to ion-probe zircon ages*. Earth and Planetary Science Letters, 128*(3), pp.373–390.

Sethuraman, J., "A constructive definition of Dirichlet priors." *Statistica sinica* (1994): 639-650.

Sharman, G. R. and Johnstone, S. A. (2017). Sediment unmixing using detrital geochronology. *Earth and Planetary Science Letters, 477*, pp.183–194.

Shuster, D.L. and Cassata, W.S., 2015. Paleotemperatures at the lunar surfaces from open system behavior of cosmogenic ^{38}Ar and radiogenic ^{40}Ar. *Geochimica et Cosmochimica Acta, 155*, pp.154-171.

Singer, B. S., Ackert Jr, R. P., and Guillou, H. (2004). $^{40}Ar/^{39}Ar$ and K-Ar chronology of Pleistocene glaciations in Patagonia. *Geological Society of America Bulletin, 116*(3-4), pp.434–450.

Sletten, V.W. and Onstott, A.T., 1998. The effect of the instability of muscovite during in vacuo heating on $^{40}Ar/^{39}Ar$ step-heating spectra. *Geochimica et Cosmochimica Acta*, *62*(1), pp.123-141.

Soĺe, J. (2014). In situ determination of K–Ar ages from minerals and rocks using simultaneous laser-induced plasma spectroscopy and noble gas mass spectrometry. *Chemical Geology, 388*, pp.9–22.

Steiger, R.H. and Jäger, E., 1977. Subcommission on geochronology: convention on the use of decay constants in geo-and cosmochronology. *Earth and planetary science letters*, *36*(3), pp.359-362.

Swindle, T., Bode, R., Boynton, W., Kring, D., Williams, M., Chutjian, A., Darrach, M., Cremers, D., Wiens, R., and Baldwin, S. (2003). AGE (Argon Geochronology Experiment): an instrument for in situ geochronology on the surface of Mars. LPI, p.1488.

Turner, G. (1968). The distribution of potassium and argon in chondrites. *In Origin and Distribution of the Elements*, (pp. 387 – 398). Pergamon.

Turner, G., 1970. $^{40}Ar/^{39}Ar$ age determination of lunar rock 12013. *Earth and Planetary Science Letters*, *9*(2), pp.177-180.

VanLaningham, S., Duncan, R. A., and Pisias, N. G. (2006). Erosion by rivers and transport pathways in the ocean: A provenance tool using $^{40}Ar/^{39}Ar$ incremental heating on fine-grained sediment. *Journal of Geophysical Research: Earth Surface, 111*(F4).

VanLaningham, S. and Mark, D. F. (2011). Step heating of $^{40}Ar/^{39}Ar$ standard mineral mixtures: investigation of a fine-grained bulk sediment provenance tool. *Geochimica et Cosmochimica Acta, 75*(9), pp.2324–2335.

Vasconcelos, P., Farley, K., Malespin, C., Mahaffy, P., Ming, D., McLennan, S., Hurowitz, J., and Rice, M. S. (2016). Discordant K-Ar and young exposure dates for the Windjana sandstone, Kimberley, Gale Crater, Mars. *Journal of Geophysical Research: Planets, 121*(10), pp.2176–2192.

Wartho, J.-A. (1991). *Argon isotope systematics and mineralogy of metamorphic hornblendes from the Karakoram* (Doctoral dissertation, University of Leeds)/

Williford, K. H., Farley, K. A., Stack, K. M., Allwood, A. C., Beaty, D., Beegle, L. W., Bhartia, R., Brown, A. J., de la Torre Juarez, M., Hamran, S.-E., et al. (2018). The NASA Mars 2020 rover mission and the search for extraterrestrial life. In From *Habitability to Life on Mars* (pp.275-308). Elsevier.

Yu, S.-Y., Colman, S. M., and Li, L. (2016). BEMMA: A hierarchical Bayesian end-member modeling analysis of sediment grain-size distributions. *Mathematical Geosciences, 48*(6), pp.723–741.

Zhan, Z.-H., Zhang, J., Li, Y., and Chung, H. S.-H. (2009). Adaptive particle swarm optimization. *IEEE Transactions on Systems, Man, and Cybernetics, Part B (Cybernetics), 39*(6), pp.1362–1381.